In-Situ Burning of Oil Spills: Mesoscale Experiments

D.D. Evans, W.D. Walton, H.R. Baum, K.A. Notarianni, J.R. Lawson,
H.C. Tang, K.R. Keydel, R.G. Rehm, D. Madrzykowski, R.H. Zile
National Institute of Standards and Technology
Technology Administration
U.S. Department of Commerce
Gaithersburg, MD 20899

and

H. Koseki
Fire Research Institute
Fire Defence Agency
Ministry of Home Affairs
Mitaka, Tokyo 181, Japan

E.J. Tennyson
Technology Assessment and
Research Branch
Minerals Management Service
U.S. Department of the Interior
Herndon, VA 22070

ABSTRACT

In 1991 a series of 14 mesoscale fire experiments were performed to measure the burning characteristics of crude oil on salt water. These oil burns in a pan ranged in size from 6 m square to 15 m square. Results of the measurements for burning rate and smoke emissions are compared to those from previous smaller scale burns conducted both in the U.S. and in Japan. The burning rate as indicated by the regression rate of the oil surface was found to be 0.055 ± 0.01 mm/s for pan fires with effective diameters greater than 7 m. Smoke particulate yields from fires greater than 2 m in diameter were found to be approximately 0.13 of the oil burned on a mass basis. Predictions of smoke plume trajectory and particulate deposition at ground level from the Large Eddy Simulation (LES) model developed as part of this research effort were found to be different from those predicted by the EPA approved SCREEN model. LES is a steady-state three-dimensional calculation of smoke plume trajectory and smoke particulate deposition based on a mixed finite difference and Lagrangian particle tracking method.

INTRODUCTION

In-situ burning of spilled oil has distinct advantages over other countermeasures. It offers the potential to convert rapidly large quantities of oil into its primary combustion products, carbon dioxide and water, with a small percentage of other unburned and residue byproducts. Burning of spilled oil from the water surface reduces the chances of shoreline contamination and damage to biota by removing the oil from the water surface before it spreads and moves. In-situ burning requires

minimal equipment and less labor than other techniques. It can be applied in areas where many other methods cannot due to lack of response infra-structure and/or lack of alternatives. Oil spills amongst ice and on ice are examples of situations where practical alternatives to burning are very limited. Because the oil is converted to gaseous products of combustion by burning, the need for physical collection, storage, and transport of recovered fluids is reduced to the few percent of the original spill volume that remains as residue after burning.

Burning oil spills produces a visible smoke plume containing smoke particulate and other products of combustion which may persist for many kilometers from the burn. This fact gives rise to public health concerns, related to the chemical content of the smoke plume and the downwind deposition of particulate, which need to be answered. Air quality is also affected by evaporation of large oil spills that are not burned. Volatile organic compounds (VOC) including benzene, toluene, and xylene and polycyclic aromatic hydrocarbons (PAH) are found in the air downwind of an evaporating crude oil spill. Laboratory measurements are useful to determine the types of chemical compounds that are expected from large oil spill burns or the evaporation of the spill. To determine the rate of emissions and the transport of the chemical compounds from a burning or evaporating spill, mesoscale experiments have been conducted outdoors using a 15 m square pan. In these experiments a layer of crude oil was discharged onto the surface of a salt water pool. The local air quality during evaporation and burning of the oil was measured.

BACKGROUND

Extensive experimental studies to quantify the capabilities of in-situ burning began in 1983 at the Oil and Hazardous Materials Simulated Environmental Test Tank (OHMSETT) facility in Leonardo, New Jersey under joint funding from the Minerals Management Service (MMS), U.S. Coast Guard (USCG), Environmental Protection Agency (EPA), and Environment Canada (EC). The primary feature of the facility was a water-filled concrete tank 203 m x 20 m x 2.4 m water depth. The tank and associated measurement and control equipment were used to evaluate the performance of oil spill response methods. In the studies conducted at OHMSETT, Prudhoe Bay, Amuligak, and several other crude oils were burned to evaluate the effects of selected physical variables including slick thickness, weathering, sea state, wind velocities, air and water temperatures, degrees of emulsification, and degrees of ice coverage on oil removal efficiency [1]. Results showed that 50 to 95 percent of all of the oils tested could be removed from the water surface by burning, as long as emulsification of the oil with water had not occurred before ignition. Ice coverage from less than 30 to 98 percent, wind speeds from calm to 26 m/s (measured 10 m above the water surface), and water temperatures from -1° to 13°C had little effect on the amount of oil removed from the water surface. Weathered, but not emulsified, oils burned with a greater percentage of removal than did the fresh oils. This was unexpected, but appeared to be a function of increased viscosity of the weathered oil [2]. These tank experiments added to the successes in removing large quantities of oil by burning in field experiments conducted by Brown and Goodman [3] and Buist and Twardus [4].

Based upon the success of these research efforts, a joint MMS and EC in-situ burning research program continued in 1985. This research program was designed to study how burning large oil spills would affect air quality by quantifying the products of combustion and developing methods to predict the downwind smoke particulate deposition. Initially, laboratory experiments were conducted by the Center for Fire Research, now the Building and Fire Research Laboratory, at the National Institute of Standards and Technology (NIST). This work sought to quantify the processes involved in oil spill combustion on open waters and in water filled channels formed in broken ice and included measurements of smoke production and prediction of smoke dispersal. Technical support from EC allowed the study to be broadened to include chemical analysis of the oil, oil residue, and oil smoke.

In the first year of the study [5] the burning process was studied at two pool diameters, 0.6 m and 1.2 m. The emission rate, size distribution, and specific extinction coefficient (relative blackness) were measured for the smoke produced by the fires. The structure of the smoke agglomerates was examined by electron microscopy. The burn residue left on the water by natural quenching of the combustion was analyzed and found to be depleted of short chain alkanes and cycloalkanes when compared with the fresh crude oil. A calculation of the induced air flow into a distribution of pool fires simulating the simultaneous burning of oil in many separate ice leads was performed to demonstrate the magnitude of the fire induced wind.

In the second year [6] extensive measurements of the PAH content of the crude oil and the smoke were performed in cooperation with Environment Canada. Measurements showed that about 10 percent of the crude oil was converted to smoke in the combustion process. A methodology was developed with which the downwind dispersal of smoke generated by one or more oil spill fires in close proximity may be predicted.

In the third year [7] smoke emission was measured during the burning of oil layers thin enough to cause boiling in the supporting water layer. Under these conditions both smoke emission and the PAH content of in the smoke were reduced compared to burning of thicker layers. The smoke yield was found to decrease by more than a factor of two when the initial oil layer thickness was decreased from 10 mm to 2 mm. Considering 18 different PAH compounds, the total PAH content in the postburn products, oil residue, smoke and vapors, was found to be less than that contained in the oil that was burned. Measurements of the optical properties and sedimentation velocities for aged and diluted smoke samples were performed. The median aerodynamic effective diameter of the smoke particulate size distribution was found to increase by 30 percent after a simulated one day of aging in a smoke plume. These characteristics are important in estimating smoke properties downwind of the oil spill fire. Analyses of smoke dispersal in the atmosphere were continued by formulating a model for smoke particle settling time which is directly related to soot deposition on the ground remote from the combustion site.

In the fourth year [8] measurements focussed on the determination of the agglomeration rate for smoke particles at both ambient temperature conditions, which corresponds to the cooler, diluted smoke in the plume and at a temperature around 100°C, which corresponds to the temperature several flame heights above the fire. Development of the plume dynamics model continued with a formulation in terms of buoyancy induced vortex trajectories (which represent the large scale plume turbulence) so that the agglomeration rate inferred from the laboratory measurements could be incorporated in the plume model. In the laboratory study the agglomerate size was observed to increase with holding time in the aging/dilution collection chamber, while in a steady state plume model, the agglomerate size will increase with downwind position along the plume.

In the fifth year [9] preparations began for the mesoscale burns to be conducted in cooperation with the USCG at their Fire and Safety Test Detachment in Mobile, Alabama. Preparation involved the development of new instrumentation to perform measurements of combustion characteristics and smoke emissions from large crude oil pan fires up to 15 meters in diameter. Many methods of transporting instrument packages into the smoke plume were investigated during the year. Testing indicated that the best method was tethered miniblimps. Efforts in the calculation of smoke plume trajectory were concentrated on developing models capable of predicting the "footprint" of soot particle deposition downwind of a burn.

In the sixth year [10,11,12] measurements were made with the newly developed instrumentation on large oil fires from 3 meters in diameter at the Fire Research Institute in Japan, to 15 meters in diameter (mesoscale) at both the Navy Fire Fighter Training facility in Norfolk, Virginia and the U.S. Coast Guard's Fire and Safety Test Detachment in Mobile, Alabama. Initial two- and three-dimensional calculations of smoke particulate transport were completed.

The effort in the seventh year of the research program was concentrated on analysis of the data from the 1991 mesoscale experiments. The initial results were the major burning characteristics of mass loss rate and fraction of the oil burned that was emitted as particulate. The extensive ground and smoke plume measurements of chemical components emitted from the oil fires remain to be analyzed fully. Additional laboratory measurements of smoke yield were performed with the identical oil used in the mesoscale experiments to examine the effect of scaling. Calculations of the smoke plume trajectory and downwind particulate deposition at ground level were completed.

EXPERIMENTAL FACILITIES

To understand the important features of in-situ burning it is necessary to perform both laboratory and mesoscale experiments. Finally, actual burns of spilled oil at sea will be necessary to evaluate the method at the anticipated scale of actual response operations. In this research program there is a continuing interaction between findings from measurements on small fire experiments performed in the controlled laboratory environments of NIST and the Fire Research Institute (FRI) in Japan, and large fire

experiments at facilities like the USCG Fire Safety and Test Detachment in Mobile, Alabama where outdoor liquid fuel burns in large pans are possible.

At NIST, two major facilities were used to perform measurements on crude oil pool fires ranging in size from 0.085 m to 0.6 m in diameter. The smallest fires, 0.085 m diameter, were conducted in the Cone Calorimeter to determine the effective heat of combustion for the crude oils and evaluate smoke yield using three different measurement methods. The Cone Calorimeter, shown in figure 1, is more formally known as Standard Test Method for Heat and Visible Smoke Release Rates for Materials and Products Using an Oxygen Consumption Calorimeter [13]. The name of the apparatus, Cone Calorimeter, is derived from the shape of the heater used to irradiate samples. The heater coils are formed along the inner surface of a truncated cone. By imposing additional thermal radiation on a small sample, the sample is made to burn as if it were in the middle of a larger fire. The major material flammability characteristics can be evaluated using this laboratory apparatus. These include: rate of heat release, effective heat of combustion, total heat release, ignitibility, mass loss rate, smoke specific extinction area, and yields of various gaseous species and particulate.

A larger calorimeter apparatus capable of accommodating samples up to 0.6 m in diameter was used to provide additional NIST laboratory data on the effect of fire diameter on smoke yield from crude oil fires. This instrumented exhaust hood shown in figure 2 has been the workhorse of the laboratory scale studies of crude oil combustion for several years in this research program [5-11]. Samples drawn from the exhaust hood duct were used to quantify the amount of each major combustion product generated per kilogram of crude oil burned, the chemical composition of the smoke including PAH content, the particulate size distribution of both fresh and aged smoke, and the oxygen consumed in the combustion process. Oxygen consumption calorimetry is used to calculate the heat release rate of the fire, which is the primary quantity used to characterize burning intensity. To further characterize the combustion process, additional instrumentation was used to measure radiant heat flux from the flame and the mass loss rate of the burning fuel.

The relatively small, 0.6 m diameter, fires provided a means of measuring fire characteristics under controlled conditions, but are too small to provide an adequate test of measurement equipment being developed for field use. Through the cooperation of the Fire Research Institute (FRI) in Tokyo, Japan, joint studies of crude oil burning characteristics were conducted. FRI maintains a fire test facility in which crude oil pools up to 3 m in diameter are burned, with all of the combustion products collected in a large hood system. Figure 3 shows a 2 m diameter crude oil fire burning in the 24 m x 24 m x 20 m high test hall. This facility could accommodate fires that are large enough so that sampling packages designed for mesoscale tests could be evaluated. The exhaust system for the building was instrumented so that measurements similar to those performed in the NIST facility could be made by effectively using the entire FRI test building as a smoke collection hood.

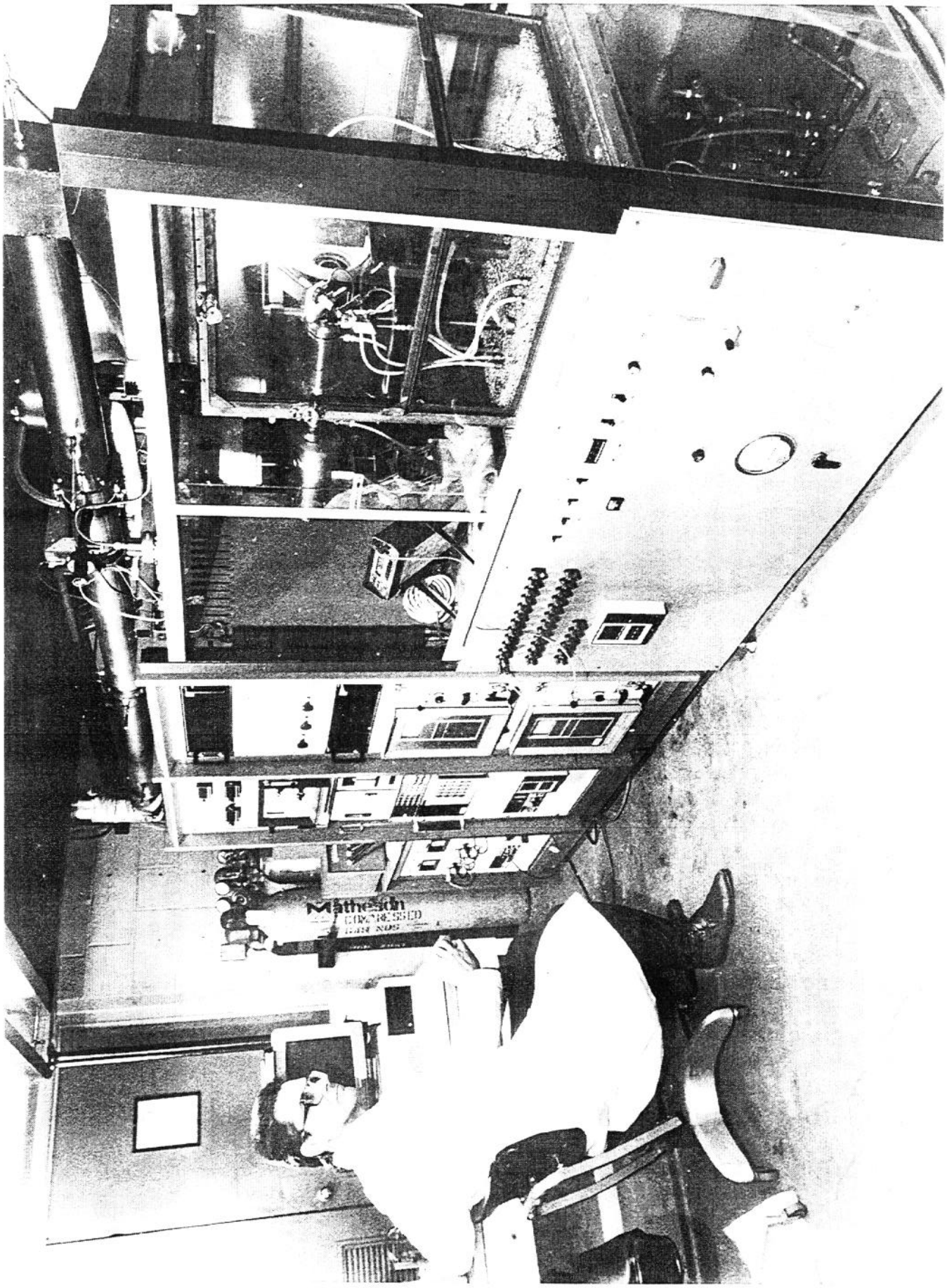

Figure 1. NIST Cone Calorimeter

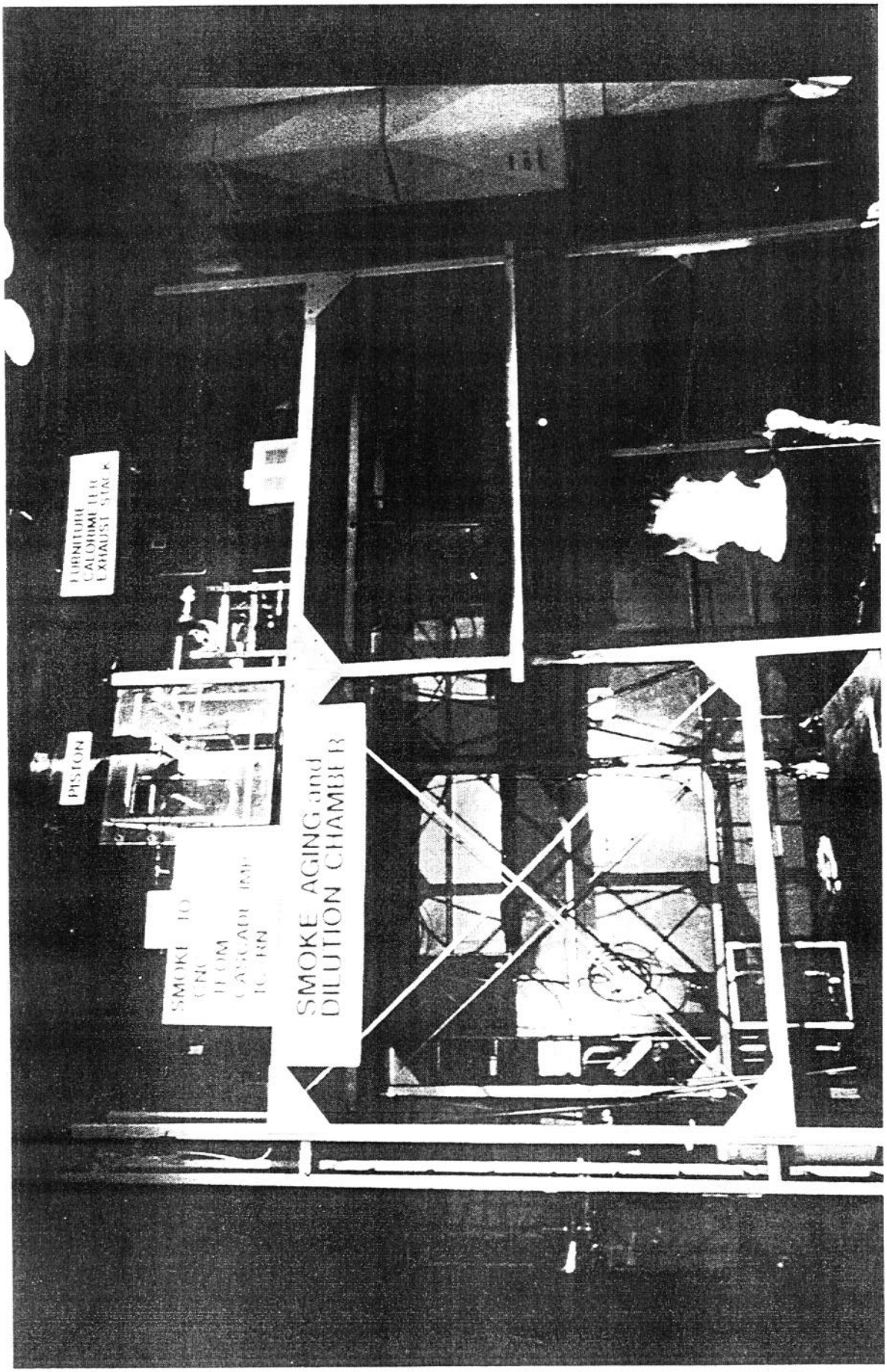

Figure 2. NIST Large Calorimeter

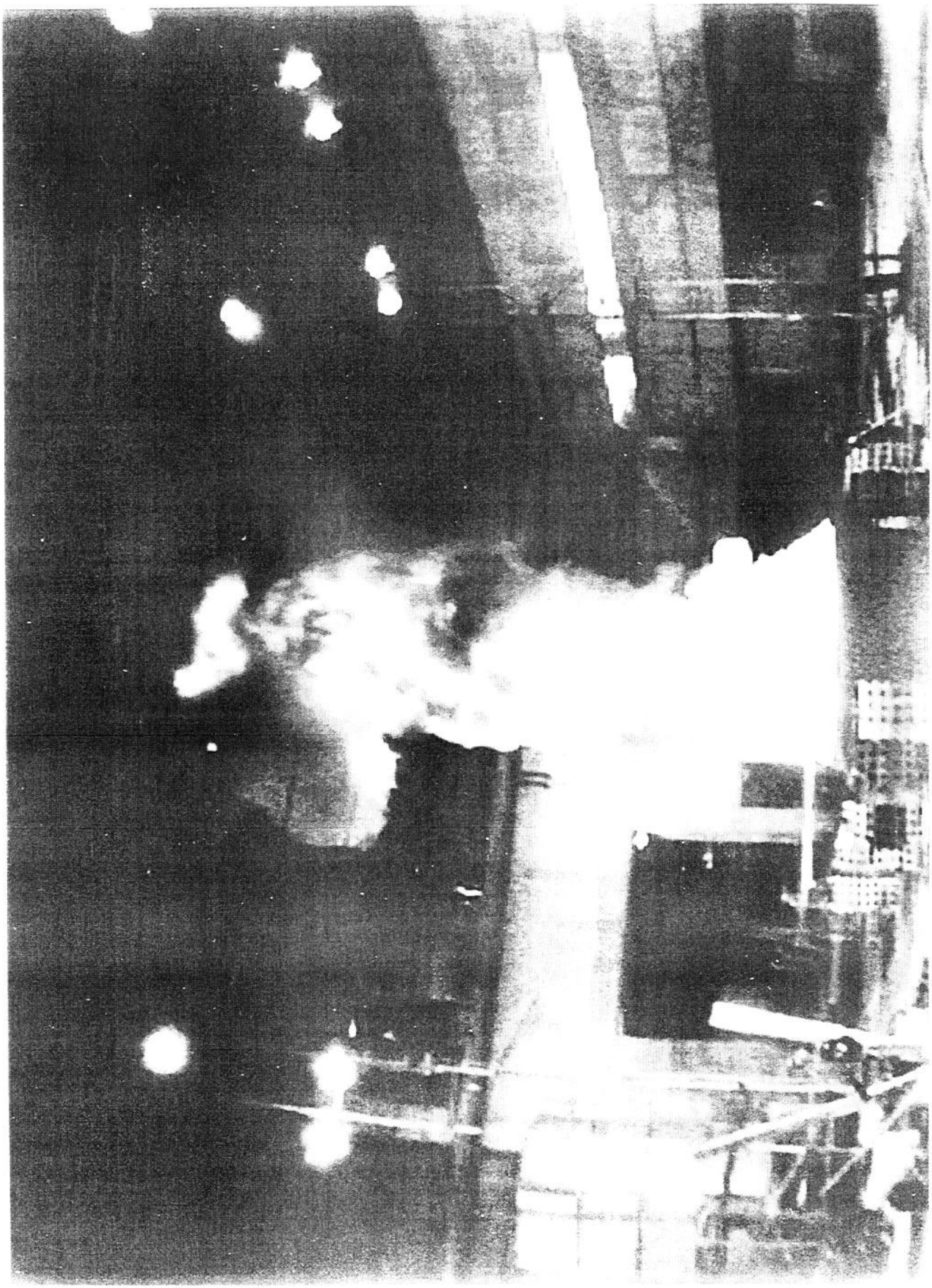

Figure 3. Two meter diameter crude oil fire at FRI

ELEMENTAL ANALYSIS OF CRUDE OILS

Two types of oil were used in this study. A Louisiana crude oil and a Murban crude oil. Samples of each oil type were analyzed for composition by a commercial laboratory. Two separate analyses were performed by the same laboratory for each oil and the average results are presented in table 1.

Table 1. Elemental analysis of Louisiana and Murban crude oils

Element	Louisiana Oil (mass fraction)	Murban Oil (mass fraction)	Repeatability
Carbon	0.862	0.848	± 0.2 %
Hydrogen	0.134	0.141	± 1.6 %
Sulfur	0.000	0.008	± 4.0 %

EFFECTIVE HEAT OF COMBUSTION

Heat is released in all combustion (oxidation) reactions. The amount of heat released per unit quantity of fuel oxidized is defined as the heat of combustion. Heat of combustion is normally determined in an ASTM D 240 oxygen bomb calorimeter, in which a known mass of fuel is burnt completely in an atmosphere of pure oxygen. In fires, however, incomplete combustion occurs resulting in the formation of carbon monoxide, smoke particles, and other incomplete combustion products. The amount of heat actually released from the fire divided by the amount of fuel burned is termed the effective heat of combustion. These two quantities were measured in the Cone Calorimeter, and the effective heat of combustion for each of the two oils used in this study was determined. The effective heat of combustion for the Louisiana oil was 41900 kJ/kg, and 42700 kJ/kg for the Murban oil. This effective heat of combustion is used in conjunction with the mass loss data for the large-scale fires to determine the heat release rate of the large fires.

MESOSCALE CONFIGURATION

The mesoscale burns of crude oil were carried out under the direction of NIST at the United States Coast Guard Fire and Safety Test Detachment facility on Little Sand Island in Mobile Bay Alabama. Little Sand Island is approximately 0.2 km^2 in size and includes three decommissioned ships docked in a lagoon. The ships and facilities on the island have been used for a wide variety of full-scale marine fire tests. Figure 4 is a photograph of a burn in progress, and figure 5 is a plan view of the portion of the island used for the oil spill burns.

The burns were conducted in a nominal 15 m square steel burn pan constructed specifically for oil spill burning. The burn pan was 0.61 m deep and was constructed

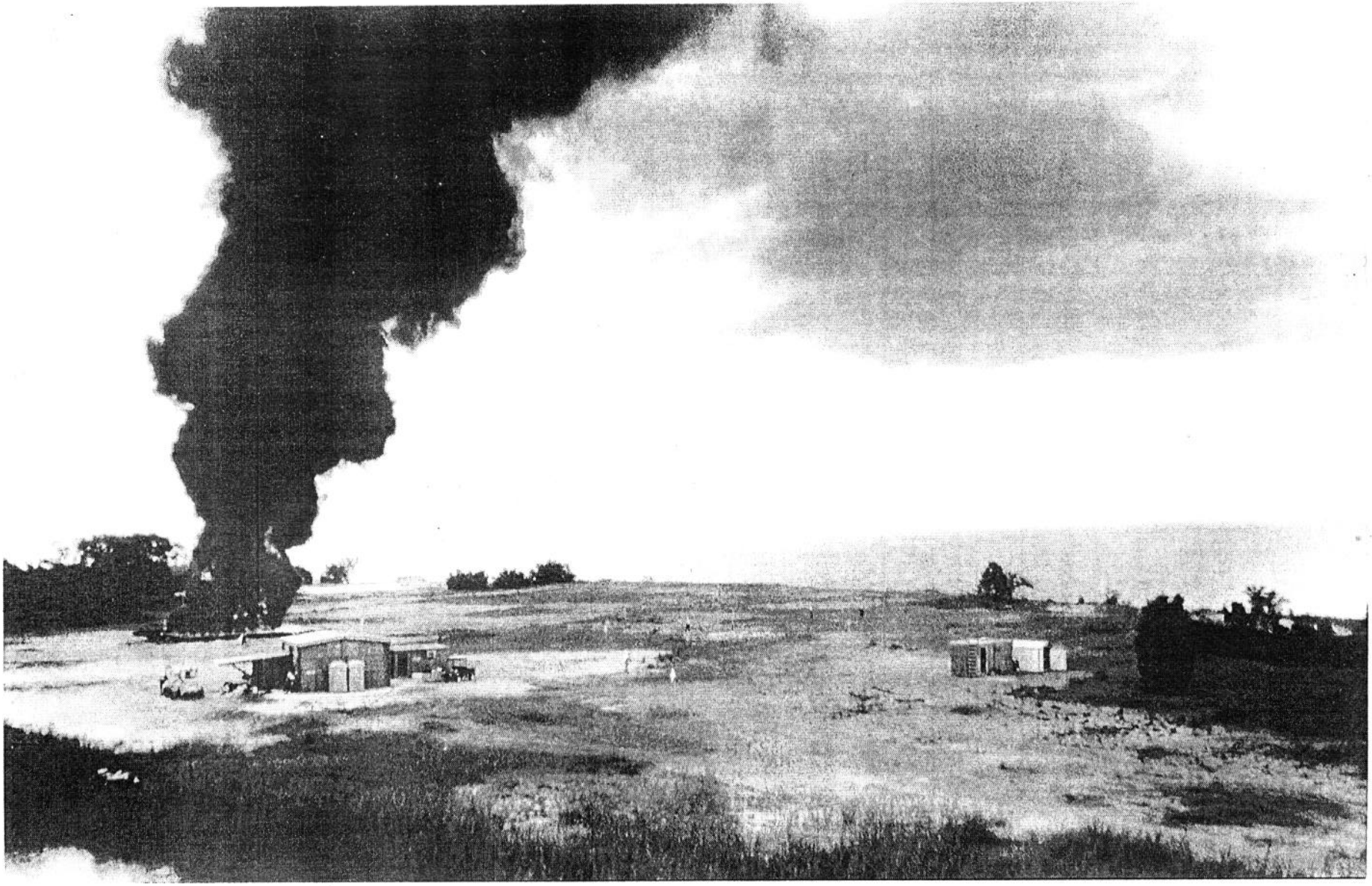

Figure 4. USCG Safety and Fire Test Detachment mesoscale burn facility in Mobile, Alabama

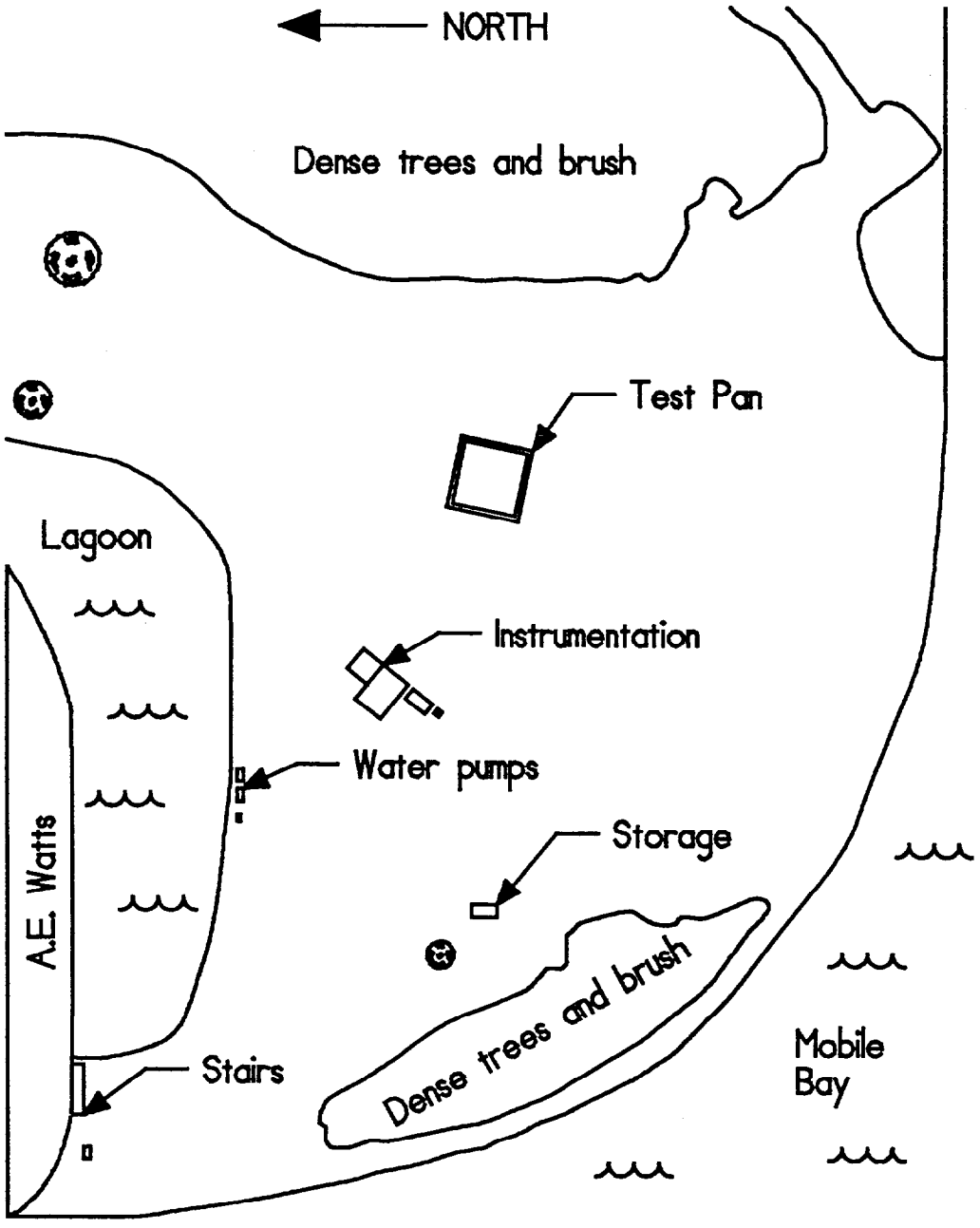

Figure 5. USCG mesoscale burn facility site plan

with two perimeter walls approximately 1.2 m apart forming an inner and outer area of the pan. The inside dimensions of the inner area of the pan were 15.2 m by 15.2 m. The two perimeter walls were connected with baffles and the space between the walls, which formed the outer area of the pan, was filled with bay water during the burns. The base of the pan was 6 mm thick steel plate and the walls were 5 mm thick steel plate. The tops of the walls were reinforced with steel angle to prevent warping during the burns. The base of the pan was located on ground level and was reinforced with steel beams on steel footers under the pan. Water fill pipes were connected to both the inner and outer areas of the pan. Water was pumped directly from Mobile Bay into both the inner and outer areas of the pan. The inner area of the pan was filled with approximately 0.5 m of water and the crude oil was added on top of the water. An oil spill containment dike approximately 0.5 m high was constructed 4 m from the outer edge of the pan.

The crude oil used in the mesoscale burns was obtained from an oil storage facility in Louisiana. The oil originated from wells in the Louisiana area and is thus referred to as Louisiana crude oil. Properties of the oil, as measured by independent oil testing laboratories, are given in table 2.

Table 2. Louisiana crude oil properties

Property	**Value (measured by independent laboratories)**
Specific Gravity	sample 1 - 0.8453 sample 2 - 0.8448
API Gravity @ 15.6°C (60°F)	sample 1 - 35.9 sample 2 - 36.0
Kinematic Viscosity @ 37.8°C (100°F)	5.49 mm^2/s (5.49 cSt)
Reid Vapor Pressure	26.9 kPa (3.9 lbf/in^2) absolute
Flash Point - Pensky Martin Closed Cup	less than ambient

Crude oil was fed to the burn pan via an underground pipe. A vertical section of the oil fill pipe penetrated the base of the pan and terminated in flanged fitting located below the water level. A plate was bolted on the flanged fitting with spacers between the plate and the flange. This allowed the oil to be injected horizontally below the surface of the water. The supply side of the oil fill pipe terminated approximately 200 m from the burn pan. Gate valves were located in the supply pipe next to the pan, 52 m from the pan and at the supply point. A check valve and a orifice plate flow meter were located in the supply pipe near the pan.

Three different primary burn areas were used in the series. These areas consisted of the full inner pan with an area of 231 m^2 and partial pan areas of 114 m^2 and 37.2 m^2. The partial pan areas were achieved by partitioning a corner of the inner pan with 0.14 m by 0.14 m timbers covered with sheet steel. Plywood skirts 0.3 m deep were attached to the timbers below the water surface to prevent the oil from flowing under the timbers.

A total of 14 mesoscale burns were conducted. These included two preliminary burns which were used to test instrumentation and procedures, 8 burns to examine the effect of burn area, and 4 burns to examine special conditions. Table 3 gives the size and areas for the mesoscale burns. An effective diameter was calculated for each of the rectangular burn areas. The effective diameter is the diameter of circle with the same area as the rectangular burn area used. The special conditions examined included the use of fire resistant boom, the effect of water spray on smoke emissions and the effect of oil aging on burning.

MESOSCALE INSTRUMENTATION

The fixed position instrumentation in and around the burn pan consisted of thermocouples in the pan, thermal heat flux gauges and instrumented steel plates facing the pan, and a manometer to measure the liquid level in the pan. The data from the thermocouples, heat flux gauges and instrumented steel plates are in the process of analysis and are not reported in this paper.

A portable array of 8 - 0.5 mm diameter bare-bead thermocouples 76 mm apart was used to determine the temperature of the water in the inner pan at two locations on opposite sides of the pan before and after the burns. The data from these thermocouples are in the process of analysis and are not presented in this paper.

A vertical manometer calibrated for water was used to measure the equivalent water level in the pan during the burns. Since the oil and the water in the pan have different densities, a correction must be applied to determine the thickness of the oil layer during the burn. A copper tube was connected to the inner pan water fill pipe on the pan side of the shutoff valve. The tube was run underground to the instrumentation building and connected to a liquid manometer. The liquid level in the manometer was videotaped during the pan fill and burn. The equivalent water level in the pan as a function of time was obtained from the videotape record.

Measurements of atmospheric conditions were made with both ground based and airborne weather stations. The ground based station was located approximately 50 m to the west of the burn pan and 3 m above the ground. The station consisted of a thermistor to measure temperature, a propeller on vane anemometer to measure wind direction and speed and a capacitive relative humidity sensor. Atmospheric data from the ground based weather station were recorded every 120 s with a computerized data acquisition system. The airborne weather station was located approximately 50 m from the pan near the ground station and was positioned for each burn to be well away from the fire plume. The airborne weather station consisted of a thermistor to

measure temperature, a cup anemometer to measure wind speed, an electronic compass to measure wind direction, and a pressure transducer to measure barometric pressure. The airborne weather station was connected to a helium filled miniblimp which was tethered approximately 50 m above the ground during the fires. Data from the airborne weather station were transmitted via radio to a ground based computerized data collection system every 20 s.

Table 3. Mesoscale burn size

Burn No.	Burn Size (m)	Burn Area		Effective Burn Diameter		Burn Area/ Full Pan Area (%)	Features
		(m^2)	(ft^2)	(m)	(ft)		
4/16	6.10 × 6.10	37.2	400	6.88	22.6	16	
4/17	6.10 × 6.10	37.2	400	6.88	22.6	16	
5/16	6.10 × 6.10	37.2	400	6.88	22.6	16	
5/17	6.10 × 6.10	37.2	400	6.88	22.6	16	
5/22	10.7 × 10.7	114	1225	12.0	39.4	49	water spray
5/23	11.9 × 15.2	181	1950	15.2	49.9	78	boom attached two ends, free to move
5/24	11.2 × 15.2	170	1830	14.7	48.2	74	boom attached two ends, free to move
5/28	8.53 × 8.53	72.8	784	9.63	31.6	32	boom attached two ends, restricted to square area
5/29	6.10 × 6.10	37.2	400	6.88	22.6	16	oil aging
5/30	10.7 × 10.7	114	1225	12.0	39.4	49	
5/31	15.2 × 15.2	231	2490	17.2	56.4	100	
6/3	10.7 × 10.7	114	1225	12.0	39.4	49	
6/4	10.7 × 10.7	114	1225	12.0	39.4	49	
6/5	15.2 × 15.2	231	2490	17.2	56.4	100	

The ground based measurements consisted of both real time measurements and samples collected for laboratory measurement. The real time measurements made both up- and downwind of the fire included total particulates and carbon dioxide, and sulfur dioxide concentrations. Filter samples were collected both upwind and downwind of the fire and analyzed in the laboratory for PAH and VOC concentra-

tions. Samples of the fresh oil before the burn, oil residue after the burn, and water in the burn pan after the burn were analyzed in the laboratory for PAH concentration. The results of the ground based measurements and laboratory analysis are not presented in this paper.

Airborne samples were collected for both laboratory analysis and analysis on the ground immediately following the burns. The sampling packages were suspended approximately 60 m below a 5.6 m long 2.3 m diameter tethered helium filled miniblimp. The miniblimp was positioned downwind from the fire with the sampling package centered in the smoke plume. The elevation and downwind position of the sampling package varied with each burn as a function of the plume position. Typically, sampling packages remained in the plume for 600 seconds which permitted an adequate sample to be collected and allowed the natural fluctuations in the plume to be averaged. Since the lift capacity of the miniblimp was limited, in general only a single sampling package could be deployed at a time. In some cases, where the burn was of sufficient duration, two packages were deployed sequentially.

The sampling packages consisted of battery powered pumps which drew samples through filters and discharged a portion of the gas into a collection bag. Filter samples were analyzed in the laboratory for PAH and VOC concentrations. Particulate size distribution was measured using a cascade impactor. In addition, smoke particulate was collected on a thermophoretic transmission electron microscope grid (TEM grid) and analyzed using a transmission electron microscope to determine particle shape. Table 4 gives a list of the airborne samples taken during the mesoscale burns. The smoke yield results will be presented in a later section. The other results from the airborne measurements are in the process of analysis and are not presented in this paper.

MESOSCALE BURN PROCEDURE

Prior to conducting a mesoscale burn, the burn size was selected and for partial pan burns the timber partitions were positioned at the appropriate location. Prior to pumping crude oil into the pan, water was pumped into the outer pan so that the water level was nearly to the top of the pan. Water was also pumped into the inner pan so that the water surface level was approximately 110 mm below the top of the pan. The distance from a reference point at the top of the pan to the surface of the water in the inner pan was measured and recorded. The temperature profile of the water in the inner pan was measured at two locations on opposite sides of the pan.

The crude oil was stored on a barge which was brought to the site prior to a burn. Oil was pumped through a flexible hose from the barge through the underground piping system and into the pan. The approximate quantity of oil delivered to the pan was monitored with an in-line flow meter. When the quantity of oil delivered to the pan approached the desired quantity, compressed air was pumped from the barge to purge the flexible hose. The barge was then disconnected from the flexible hose and the barge departed the site. The distance from the surface of the oil to the fixed reference point at the top of the pan was recorded and an oil sample was taken. The fixed position and ground based instrumentation and data recording were started and

the oil was easily ignited with an extended propane torch. Video cameras were used to record the burn.

Table 4. Mesoscale Airborne Samples

Burn No.	Miniblimp		Start Time (s)	Total Time (s)	Range (m)	Alti-tude (m)
	No.	Samples				
4/16	1.1	PAH, TEM grid	29	425	61	128
	1.2	smoke yield	1165	245	61	128
4/17	1.1	Formaldehyde, charcoal tube	17	529	61	56
	1.2	PAH, TEM grid	641	226	61	56
5/16	1	PAH	48	1273	56	44
5/17	1	smoke yield	215	681	106	100
5/22	1	smoke yield	107	403	83	38
5/23	1	PAH	--:--	617	48	30
5/28	1.1	quartz filter #1	-10	248	87	45
	1.2	quartz filter #2	436	163	87	45
5/29	1	smoke yield	155	692	47	16
5/30	1	impactor, TEM grid	0	1152	87	45
	2.1	quartz filter	28	210	87	45
5/31	2.1	quartz filter	20	429	103	150+
6/3	1	PAH, charcoal tube	32	1515	109	150+
	2	smoke yield	71	722	109	150+
6/4	1.2	PAH, impactor	387	948	109	160
	2	formaldehyde, charcoal tube, passive filter	12	1351	109	160
6/5	1.1	smoke yield, TEM grid	59	915	100	121
	1.2	PAH, charcoal, passive filter	1134	868	100	121
	2	PAH, passive filter	109	1883	100	121

Note: All times from ignition

When the flames were no longer visible, the temperature profile of the water in the inner pan was measured at two locations on opposite sides of the pan. The distance from the surface of the water/oil residue to the fixed reference point at the top of the pan was recorded and a burn residue sample was taken. The residue was collected with absorbent material and placed in drums for disposal. The quantity of residue was estimated from the volume of the drums filled taking into account the absorbent material and water collected. After four of the burns (5/30, 5/31, 6/3, and 6/5), there was a greater quantity of residue than could be readily collected in two or three drums. It is estimated that there was two to three times the quantity of residue found in the earlier burns due to variations in the extinction process. In these cases after the residue had cooled, a small quantity of diesel fuel was poured on the residue and the diesel and burn residue mixture was ignited. This procedure was repeated up to three times until the residue had been reduced to a manageable quantity. The residue was then collected and measured.

The water spray system used in burn 5/22 was designed by Alaska Clean Seas[1] to examine the effect of water spray on smoke production. Twelve nozzles which produced an umbrella like spray pattern were located approximately 1 m above the fuel surface. Bay water was pumped to the nozzles starting 83 seconds after ignition with a nozzle pressure of 34 kPa. At 373 s after ignition the pressure was increased to 69 kPa, at 507 s the valve to the spray system was closed and the spray terminated at 540 s.

For the oil aging burn 5/29 the oil was pumped in the pan at 0812 hours local time and the burn started at 1627 hours local time. The oil remained on the surface of the pan for a total of approximately 29700 s prior to ignition.

MESOSCALE RESULTS

Table 5 gives a summary of the meteorological conditions measured during each of the burns. The values in the table are averages over the time from ignition to extinction. Wind directions are the direction from which the wind originates with 0° being north. Although the measurements were taken at a single ground and single airborne location and there was some variation in the meteorological conditions during the burns, the burns were of relatively short duration and the averages are representative of the actual conditions. Before and after the burns, profiles of the meteorological conditions were made with the airborne weather station up to an elevation of 100 m. The profiles showed the meteorological conditions to be generally uniform above 20 m.

---

[1] Certain commercial equipment, instruments, materials, or methods are identified in this paper in order to specify the experimental procedure adequately. Such identification is not intended to imply recommendation or endorsement by the National Institute of Standards and Technology, nor is it intended to imply that the materials or methods used are necessarily the best available for the purpose.

Table 5. Mesoscale meteorological conditions

Burn No.	Ground Weather Station					Airborne Weather Station			
	Wind Speed. (m/s)	Wind Dir. (°)	Temp. (°C)	R.H. (%)	B.P. (kPa)	Alt. (m)	Wind Speed (m/s)	Wind Dir. (°)	Temp. (°C)
4/16	1.5	117	25.3	74	101.9	NA	NA	NA	NA
4/17	1.9	150	24.0	73	101.6	NA	NA	NA	NA
5/16	2.1	141	27.0	81	101.4	50	5.3	150	25.2
5/17	1.7	165	26.3	69	101.5	50	3.9	141	25.2
5/22	4.0	57	24.3	87	101.3	NA	NA	NA	NA
5/23	5.0	107	25.3	85	NA	NA	NA	NA	NA
5/24	2.4	134	25.9	89	NA	51	6.0	120	24.3
5/28	1.2	206	27.5	92	101.8	48	4.1	189	25.3
5/29	5.0	189	30.1	72	101.6	41	9.8	196	26.0
5/30	3.9	168	28.7	72	101.5	48	6.2	168	25.6
5/31	0.8	40	27.3	81	101.4	52	1.3	49	24.5
6/3	1.0	61	26.4	74	NA	NA	NA	NA	NA
6/4	2.1	177	30.2	72	NA	NA	NA	NA	NA
6/5	2.1	41	30.3	69	NA	NA	NA	NA	NA

NA - not available

BURNING RATE

The burning of the crude oil was observed to take place in four distinct phases. The four phases were; 1) spreading, 2) steady burning, 3) steady burning with boiling of the water below the oil layer, and 4) transition to extinction. The spreading phase lasted a relatively short period of time as flames spread on the surface from the single ignition point on the upwind side of the pan to cover the entire fuel surface. Once the entire oil surface was covered with flames, the burning continued at a steady rate until the water below the oil surface began to boil. The onset of boiling was characterized by a noticeable increase in sound and bubbles breaking through the oil surface. During boiling the burning rate increased to a steady rate which was greater than the rate prior to boiling. When the fuel was nearly consumed, the fire began a transition to extinction. This was characterized by areas of the oil surface with no visible

flames. Frequently, there were oscillations in the burning behavior with increased and decreased burning area and transition to and from boiling. The burning area decreased toward the downwind side of the pan until extinction. A brief chronology of the observed burning behavior for each of the burns is given in table 6.

Table 6. Mesoscale burn chronology

Burn No.	Effective Burn Dia. (m)	Initial Oil Depth (mm)	Time to Full Involve-ment (s)	Time to Begin Boiling (s)	Time to Begin Extinction (s)	Time to Extinction (s)
4/16	6.88	90	40	663	1588	1673
4/17	6.88	43	20	564	671	812
5/16	6.88	34	30	1008	1186	1270
5/17	6.88	60	13	850	1135	1267
5/22	12.0	32	62	NA	466	855
5/23	15.2	18	104	220	423	700
5/24	14.7	33	85	270	630	1203
5/28	9.63	31	38	387	486	613
5/29	6.88	62	241	761	1186	1455
5/30	12.0	51	42	591	1035	1082
5/31	17.2	49	15	596	950	1068
6/3	12.0	63	27	825	1215	1251
6/4	12.0	61	47	654	769	1200
6/5	17.2	62	32	641	855	2465

Note: All times from ignition

The average burning rate or the rate at which the oil was consumed during burning was estimated from the burn time and the quantity of oil. For the burns where the manometer operated satisfactorily, the average rate, as well as the rates prior to boiling and during boiling were calculated.

For all burns except the preliminary burn 4/16, the quantity of the oil was determined from the difference in the elevation of the water surface before the oil was added to the pan and the elevation of the oil surface in the pan. For the full pan burns the

difference in elevation provided a direct measurement of the quantity of oil added to the pan. For the partial pan burns, as oil was added to the confined area of the pan the water level in the unconfined area changed since water was free to flow under the timbers or boom used for containment. The hydrostatic head from the water and the oil in the confined area would equal the hydrostatic head from the water in the unconfined area. Equating the hydrostatic heads in the two areas of the pan yields the following expression for the change in the thickness of the oil layer in the confined area of the pan.

$$\Delta h_O = \frac{\Delta h_{O,W}}{1 - \left(\frac{A_T - A_O}{A_T}\right)\Gamma} \qquad (1)$$

where:

Δh_O = change in oil layer thickness in the partial pan area (m)
$\Delta h_{O,W}$ = change in the combined oil layer and water thickness in the partial pan area (m)
A_T = total pan area (m^2)
A_O = partial pan area (m^2)
Γ = the ratio of the specific gravity of the oil to the specific gravity of water

For the manometer readings, the measured equivalent water level was converted to oil depth and smoothed using a running 13 point (200 s) running average. The oil surface regression rate was calculated using a least squares linear fit over the time for both the steady burning and steady burning with water boiling phases. The average surface regression rate over the total steady burning phase was determined using a linear fit from the point at which steady burning began to the point at which the transition to extinction began. The specific mass burning rate (rate of mass loss per unit area) was calculated from the surface regression rate and the density of the oil. The heat release rate was determined by multiplying the mass loss rate by the effective heat of combustion for the crude oil (41.9 MJ/kg).

Table 7 gives the initial volume of oil, the volume of residue collected, the volume of oil consumed by burning and the percentage of the initial volume of oil consumed by burning. In the cases where the residue was burned before cleanup the number and duration of the residue burns is shown. The oil consumed includes the total oil consumed during both the primary and residue burns. When burning oil is confined in a towed boom, the oil residue is maintained at a sufficient thickness to support burning. The percent of oil consumed during the mesoscale burns is therefore representative of the percent which would be expected to be consumed if the oil were in a towed boom.

Table 7. Mesoscale oil volume

Burn No.	Crude		Residue		Consumed		Consumed (%)	Residue burns
	(m^3)	(gal)	(m^3)	(gal)	(m^3)	(gal)		
4/16	3.36[1]	887	0.23	60	3.13	827	93	
4/17	1.60	423	0.10	25	1.50	398	94	
5/16	1.30	343	0.33	88	0.97	255	75	
5/17	2.25	594	0.17	44	2.08	550	92	
5/22	3.37	969	0.12	32	3.25	937	96	
5/23	3.31	875	0.33	88	2.98	787	90	
5/24	5.56	1470	0.12	30	5.44	1440	98	
5/28	2.25	594	0.16	41	2.09	553	93	
5/29	2.31	610	0.21	55	2.1	555	91	
5/30	5.80	1530	0.07	18	5.73	1510	99	1st - 1318 s 2nd - not recorded
5/31	11.8	3110	0.16	43	11.6	3065	99	1st - 1054 s 2nd - 460 s
6/3	7.22	1910	0.10	26	7.12	1880	99	1st - 769 s 2nd - 304 s 3rd - 401 s
6/4	6.98	1845	0.30	81	6.68	1765	96	
6/5	14.1	3720	0.14	37	14.0	3680	99	456 s

[1] Estimated from flow meter

Note: Residue quantities after residue burns if applicable

Table 8 shows the average burning rate and surface regression rates based on the measurements of the oil surface level in the pan and the observed burn times. Table 9 gives the same information in engineering units. Figure 6 is a graph of the average surface regression rate as a function of the effective burn diameter. From this graph it appears that for the range of diameters used in the mesoscale burns there is no dependency of surface regression rate on burn area. With the exception of the burn with a regression rate of 0.023 mm/s (5/16) and the burn with water spray (5/22) the mean value is 0.055 ± 0.01 mm/s. The rate of 0.023 mm/s is most likely due to measurement error. The mean value for the burning rate per unit area is 0.047 ± 0.01 $kg/s/m^2$ (4.9 ± 1 $gal/hr/ft^2$) and for the heat release rate per unit area is 1950 ± 300 kW/m^2. The scatter in the regression, burning and heat release rates was due in part to the variable nature of the burns. The wind direction and speed contributed to the

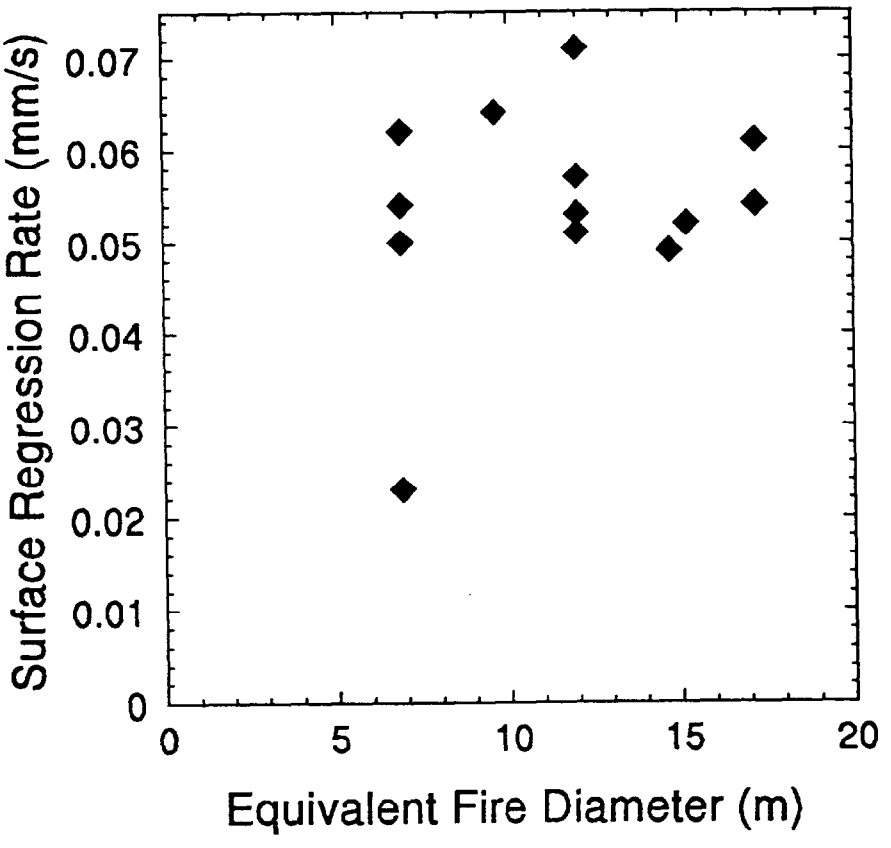

Figure 6. Mesoscale average surface regression rate

wide variation in extinction behavior observed although it did not appear to affect the average burning rate. In some cases there was a rapid transition from full pan involvement to extinction. In other cases the fire would approach extinction with as little as 5% of the fuel surface covered by flames then return to full involvement. In some cases the wind would corral the remaining fuel in a corner of the pan as the fire approached extinction allowing a significant fraction of the oil to be consumed.

Table 8. Mesoscale average burning rate

Burn No.	Effective Burn Dia. (m)	Burn Time (s)	Oil Consumed		Average Burning Rate			Average Surface Regression Rate
			(kg)	(m^3)	($kg/s/m^2$)	(kW/m^2)	MW	(mm/s)
4/16	6.88	1548	2645[1]	3.13	0.046	1925	72	0.054
4/17	6.88	651	1270	1.50	0.052	2195	82	0.062
5/16	6.88	1156	820	0.97	0.019	799	30	0.023
5/17	6.88	1122	1760	2.08	0.042	1765	66	0.050
5/22	12.0	404	2745	3.25	0.060	2500	285	0.071
5/23	15.2	319	2520	2.98	0.044	1825	331	0.052
5/24	14.7	645[2]	4600	5.44	0.042	1755	299	0.049
5/28	9.63	448	1765	2.09	0.054	2270	165	0.064
5/29	6.88	1045[3]	1775	2.10	0.046	1910	71	0.054
5/30	12.0	993	4840[4]	5.73	0.043	1790	204	0.051
5/31	17.2	935	9800[4]	11.6	0.045	1900	439	0.054
6/3	12.0	1188	6015[4]	7.12	0.044	1860	212	0.053
6/4	12.0	1020[2]	5645	6.68	0.049	2030	232	0.057
6/5	17.2	1000[2]	11830[4]	14.0	0.051	2145	496	0.061

[1] Estimated from flow meter
[2] Effective burn time due to long-term intermittent burning at end of the burn
[3] Effective burn time due to slow initial fire spread
[4] Residue was burned

Burn 5/22 which was the burn with water spray showed a slightly higher burning rate than the rest of the burns. When the water spray was initiated it appeared that water reached the surface and the sound was similar to that heard during boiling for the

other burns. It is possible that boiling of the water spray on the fuel surface may have enhanced the burning.

The burning rate from the aged oil was nearly same as the average for the fresh oil. This would indicate that short term aging does not effect burning rate.

Table 9. Mesoscale average burning rate (engineering units)

Burn No.	Effective Burn Dia. (ft)	Burn Time (s)	Oil Consumed (gal)	Initial Oil Thickness (in)	Average Burning Rate (gal/hr/ft^2)	Average Surface Regression Rate (in/min)
4/16	22.6	1548	827[1]	3.5	4.8	0.13
4/17	22.6	651	398	1.7	5.4	0.15
5/16	22.6	1156	255	1.4	2.0	0.05
5/17	22.6	1122	550	2.4	4.4	0.12
5/22	39.4	404	937	1.3	6.3	0.17
5/23	49.9	319	787	0.7	4.6	0.12
5/24	48.2	645[2]	1440	1.3	4.4	0.12
5/28	31.6	448	553	1.2	5.6	0.15
5/29	22.6	1045[3]	555	2.4	4.8	0.13
5/30	39.4	993	1510[4]	2.0	4.5	0.12
5/31	56.4	935	3065[4]	1.9	4.7	0.13
6/3	39.4	1188	1885[4]	2.5	4.6	0.13
6/4	39.4	1020[2]	1765[4]	2.4	5.1	0.13
6/5	56.4	1000[2]	3680[4]	2.4	5.3	0.14

[1] Estimated from flow meter
[2] Effective burn time due to long-term intermittent burning at end of the burn
[3] Effective burn time due to slow initial fire spread
[4] Residue was burned

The burn time used to compute the average burning and surface regression rates was the time from full pan involvement to the beginning of extinction. For burns where an extended period of transition to extinction burning was observed (5/24, 6/4, and 6/5), the effective time of steady burning was adjusted to account for the additional burning during the transition phase. Burn 5/29 exhibited particularly slow initial fire

spread and the steady burn time was adjusted to compensate for the oil consumed during that time period.

After completion of all of the burns, the flow meter in the oil transfer line to the pan was found to have been fouled with a piece of foreign matter. The measurements from the flow meter were not used to calculate the burning rate except for burn 4/16. Complete oil surface level measurements were not available for this burn so the volume of fuel was estimated using the flow meter measurements and a correction based on the flow meter measurement for burn 4/17.

Table 10 gives the oil surface regression rate determined from the measurements of the oil surface level and determined from the manometer. In addition, the surface regression rates before and during boiling as determined from the manometer are given. The regression rates determined from the fuel surface measurements are within 6% of the average rates determined from the manometer. The agreement indicates that the methodology used to determine the regression rates from the surface level measurements and the steady burning duration provides good results within the overall accuracy of field experiments. The observation that the regression rates from the surface level measurements are slightly higher than those from the manometer is an indication that a small amount of the fuel was consumed before and after the steady burning period.

Table 10. Mesoscale average oil surface regression rate

Burn No.	Effective Burn Dia. (m)	Burn Time (s)	Oil Consumed (kg)	Surface Regression Rate			
				From Manometer			From Fuel Level
				Before Boiling (mm/s)	During Boiling (mm/s)	Average (mm/s)	Average (mm/s)
5/31	17.2	935	9800[2]	0.045	0.060	0.051	0.054
6/3	12.0	1188	6015[2]	0.049	0.061	0.053	0.053
6/5	17.2	1000[1]	11830[2]	0.054	0.073	0.059	0.061

[1] Effective burn time due to long-term intermittent burning at end of the burn
[2] Residue was burned

Figure 7 shows the average, before boiling and during boiling surface regression rates from the manometer measurements. It can be seen that the burning rate during boiling increased approximately 30% from the burning rate before boiling. This phenomenon has been observed in laboratory experiments and is due to the increased mixing and volatilization of the fuel caused by the boiling of the water under the fuel surface. Also shown in figure 7 are the results from some smaller scale burns which will be discussed in the next section.

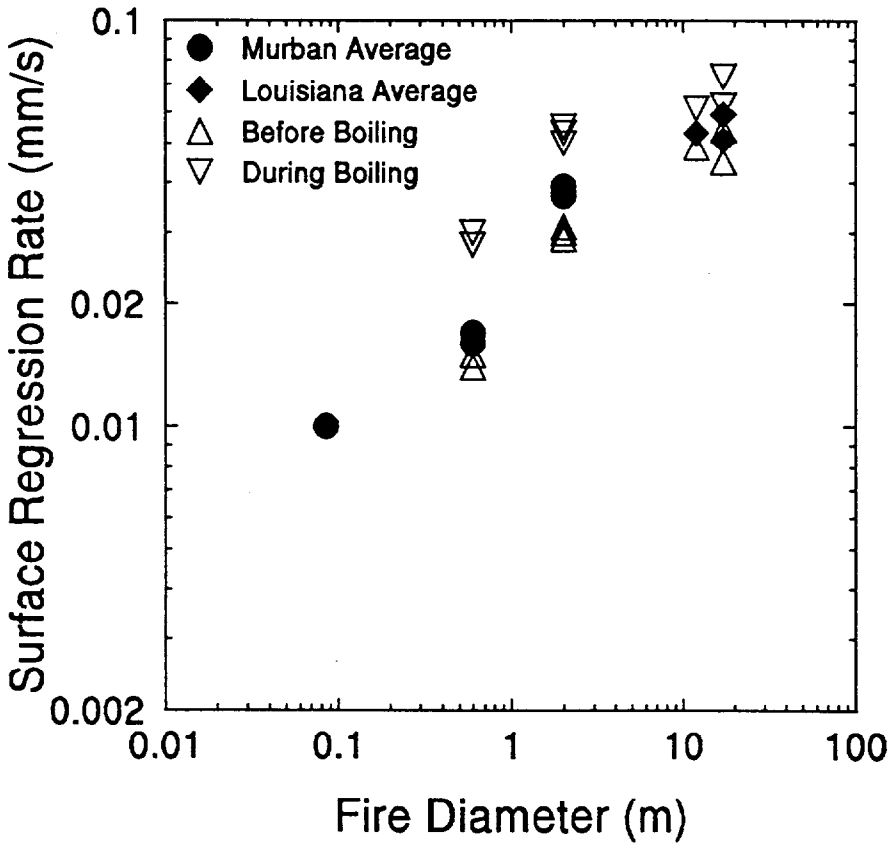

Figure 7. Average surface regression rate (all scales)

BURNING RATE -- EFFECT OF SCALE

Burning rates were measured for pool fires with diameters in the range of 0.085 m to 2 m. These pool fires, after an initial ignition transient, achieved nearly steady burning conditions. Over this range of pool fire diameters, there is a strong increase in burning rate with increasing diameter. This reflects a change from convection-dominated heating of the fuel for the 0.085 m diameter fire to radiation-dominated heating for the larger diameter fires.

Table 11. Laboratory measurements of burning rate for Murban crude oil

		Burning Rate ($kg/s/m^2$)			Surface Regression Rate (mm/s)		
		Before Boiling	During Boiling	Burn Avg.	Before Boiling	During Boiling	Burn Avg.
Cone Calorimeter D = 0.085 m		NA	NA	0.0082	NA	NA	0.01
Large Calorimeter D = 0.6 m	1	0.017	0.034	0.020	0.014	0.028	0.016
	2	0.018	0.035	0.020	0.015	0.030	0.016
	3	0.018	0.035	0.021	0.015	0.030	0.017
FRI, Japan D = 2.0 m	1	0.037	0.066	0.044	0.031	0.055	0.037
	2	0.035	0.060	0.045	0.030	0.050	0.038
	3	0.035	0.063	0.047	0.029	0.053	0.039

NA - not available, fire extinguished prior to boiling

The study of crude oil combustion on water is complicated by two factors. One is that the oil is being burned in a layer floating on water. The other is that crude oil is a blend of many hydrocarbons with a wide range of boiling points the majority of which are at greater temperatures than the boiling point of water. Distillation measurements of the Louisiana crude oil show that 90 percent of the compounds in the oil have boiling points above 100°C. During burning the surface of the crude oil maintains a temperature of around 300°C. As the fuel is consumed, heat transferred through the fuel to the water below can result in boiling of the water. The boiling effect has been observed in laboratory scale as well as field scale burns. Boiling of the water below the fuel agitates the fuel layer with both fuel and water droplets being sprayed into the flame, substantially increasing the burning rate of the fire. Burning rates are thus reported prior to and during the boiling phase.

Burning and surface regression rates for the Murban crude oil are presented in table 11 and heat release rates in table 12. The burning rate was determined from the mass

of fuel consumed, which was recorded as a function of time, and the duration of burning. The initial oil thickness was 10 mm for the 0.085 m diameter burns, 15 mm for the 0.6 m diameter burns and 25 mm for the 2.0 m diameter burns. From the burning rate, the heat release rate of the fire was calculated by multiplying the mass loss rate of the fuel by the effective heat of combustion of the fuel as described above. The burning rate for the 0.085 m fires was 0.0082 kg/s/m^2, the surface regression rate was 0.01 mm/s and the heat release rate was 350 kW/m^2. For the accuracy indicated, identical results were obtained in four different burns with Murban oil as well as three burns with Louisiana oil.

Table 12. Laboratory measurements of heat release rate for Murban crude oil

		Heat Release Rate					
		Before Boiling		During Boiling		Burn Average	
		kW/m^2	kW	kW/m^2	kW	kW/m^2	kW
Cone Calorimeter D = 0.085 m		NA	NA	NA	NA	350	2
Large Calorimeter D = 0.6 m	1	615	174	1200	339	697	197
	2	647	183	1260	356	697	197
	3	647	183	1260	356	736	208
FRI, Japan D = 2.0 m	1	1310	4100	2290	7200	1560	4900
	2	1240	3900	2100	6600	1590	5000
	3	1210	3800	2230	7000	1640	5150

NA - not available, fire extinguished prior to boiling

The 0.6 m diameter burns were conducted in the NIST large calorimeter, and the 2.0 m diameter burns in the FRI facility. For the 0.6 m diameter burns the average burning rate over the entire burn was 0.020 kg/s/m^2, the average surface regression rate was 0.016 mm/s, and the average heat release rate was 710 kW/m^2. For the 2.0 m diameter burns the average burning rate over the entire burn was 0.045 kg/s/m^2, the average surface regression rate was 0.038 mm/s, and the average heat release rate was 1600 kW/m^2.

Figure 7 shows the surface regression rates before boiling, during boiling and the average over the entire burn. It can be seen that the surface regression rate during boiling was double the rate before boiling for the 0.6 m diameter burns and nearly double for the 2.0 m diameter burns. From figure 7 it appears that boiling resulted in a greater increase in regression rate at the smaller scales. This may be a function of the, oil type, initial oil and water thickness, and other parameters in addition to scale.

SMOKE YIELD MEASUREMENTS

The quantity of smoke produced from a fire may be expressed as a smoke yield which is defined as the mass of smoke particulate produced from burning a unit mass of fuel. Techniques now exist to measure smoke yield both in the laboratory and in the field.

Three methods were used to determine smoke yield; 1) the flux method, 2) the carbon balance method, and 3) the light extinction method. These methods are discussed in detail by Mulholland, et. al [14], and summarized below. The flux method for determining smoke yield consists of measuring the mass of smoke particulate, m_s, collected on a filter, the mass loss of the fuel burned, m_f, and the ratio of the mass flow of air through the exhaust stack to the mass flow through the filter sample, ϕ. The smoke yield calculated by the flux method is termed ε_1, and is given by the expression

$$\varepsilon_1 = (m_s/m_f)\ \phi \tag{2}$$

The carbon balance method is based on a partial carbon balance, and is the only smoke yield measurement method that can be used both in the laboratory and in the field because it does not require measurement or knowledge of the total combustion product flow. In this method, smoke yield is expressed as the product of the measured fraction of carbon in the fuel, f_c, and the ratio of the measured carbon in the form of smoke particulate to the total carbon mass in the combustion products (CO_2, CO, and smoke aerosols), Y_s. Smoke yield by carbon balance method is denoted by ε_2 and given by

$$\varepsilon_2 = f_c\ Y_s \tag{3}$$

The application of the carbon balance method to smoke yield measurements assumes that in the portion of the combustion product flow from which samples are drawn, both the smoke particulate and gaseous combustion products have been transported together from the combustion zone and their concentrations have been equally diluted by entrained air.

A smoke yield measurement that is completely independent of particulate collection on filters is the light extinction method. This method is based on determining the mass concentration of smoke particulates in a known flow rate of combustion products by measurement of visible light attenuation over a known path length. In this study smoke attenuation measurements were made with a laser photometer. The design of the instrument is described by Babrauskas and Mulholland in reference [15]. The light source used in the instrument is a helium-neon laser with a low flow rate air purge to avoid deposition of soot on the optics. Detector electronics processed the signal and the output was recorded directly in units of extinction coefficient, k (m^{-1}). Calibration was accomplished with known neutral density filters introduced in the beam.

As part of the laboratory measurements in the NIST large calorimeter, the assumption that both gaseous and particulate combustion products were drawn together with entrained fresh air into the hood exhaust from which samples were drawn was checked during the burning of 0.6 m diameter crude oil fires. Visual observation indicated all of the smoke particulate was collected by the hood. Concentrations of CO_2, the major gaseous combustion product from crude oil fires were measured along all of the open areas surrounding the hood. These measurements showed that the concentration of CO_2 was not above ambient anywhere on the perimeter of the apparatus. It was concluded that all combustion products from the fires were being drawn into the hood. Samples for analysis were drawn from the exhaust stack sufficiently downstream of the hood inlet to assure uniform mixing.

In the field, smoke was drawn by a battery operated pump through a pre-weighed filter which collected the particulates. The clean gas passed through the pump to a set of micrometer adjusted flow control valves which metered and diverted a portion of the gas flow to a 5 liter sample collection bag. A radio controlled switch was used to start and stop the pump remotely as the sampling package was carried into and removed from the fire plume [11]. The filter samples were weighed on a precision balance after the burn and the concentrations of CO_2 and CO in the sample collection bag were determined using a gas chromatograph. In the mesoscale burns, the sampling package was suspended below a tethered miniblimp and was manually maneuvered from the ground and held in the smoke plume downwind of the fire. The altitude and range from the fire are given in table 4. The sample collection times were nominally 600 seconds.

Smoke yield measurements for the two crude oils, Murban and Louisiana, using all three measurement methods in laboratory experiments are presented in table 13. From table 13 it can be seen that there is excellent agreement between all three methods in the Cone Calorimeter. The largest variation between the three methods is 6%. This is most likely because the Cone Calorimeter produces a highly controlled and reproducible fire environment. The smoke yield from the Louisiana crude oil is approximately 20% greater than the yield from the Murban crude oil. This may be due in part to the slightly high carbon content in the Louisiana oil as shown in table 1. The largest variation between the three methods was 43% for the 0.6 m diameter fires and 17% for the 2.0 m diameter fires. This reflects the difficulty of reproducing larger scale fires.

Table 13. Laboratory measurements of smoke yield from crude oil fires

		Fuel Type	Flux Method ε_1	Carbon Balance Method ε_2	Light Extinction Method ε_3
Cone Calorimeter D = 0.085 m	1	Murban	0.053	0.053	0.053
	2	Murban	0.052	0.052	0.049
	3	Murban	0.057	0.057	0.054
	4	Murban	0.054	0.056	0.052
	5	Louisiana	0.063	0.067	0.060
	6	Louisiana	0.058	0.062	0.061
	7	Louisiana	0.063	0.068	0.062
Large Calorimeter D = 0.6 m	1	Murban	0.093	0.080	0.067
	2	Murban	0.093	0.077	0.082
	3	Murban	0.090	0.082	0.063
FRI, Japan D = 2.0 m	1	Murban	0.134	0.139	0.149
	2	Murban	0.128	0.137	0.150

Smoke yields from the mesoscale burns are given in table 14 and smoke yields calculated by the carbon balance method for all scale are shown in figure 8. For the mesoscale burns an estimation of the uncertainty of the smoke yield was determined. The uncertainty interval was based on the accuracy of the balance, the chromatograph and the flow measurements. The uncertainty is shown as error bars in figure 8. From figure 8 it can be seen that smoke yield is dependent on scale. The yield is lower for smaller diameter fires and appears to reach a plateau of approximately 0.13 for fires with diameters above 2 m. In small diameter fires the air which is entrained around the fire perimeter more readily mixes with the fuel resulting in more complete combustion and a lower smoke yield.

The smoke yield from burn 5/17 is distinctly lower than the yields from the other burns. An examination of the start time, sample duration, wind speed and burning rate did not provide an explanation for the low result. The smoke yield for the burn with water spray was less than the yield from four of the burns but greater than the yield from one of the burns. The results are inconclusive and at best the water spray might have reduced the smoke yield slightly, although there was no noticeable difference in smoke production during the burn. Although the smoke yield from the aged oil was on the high side of the values, a definite conclusion concerning the smoke yield from aged oil cannot be reached.

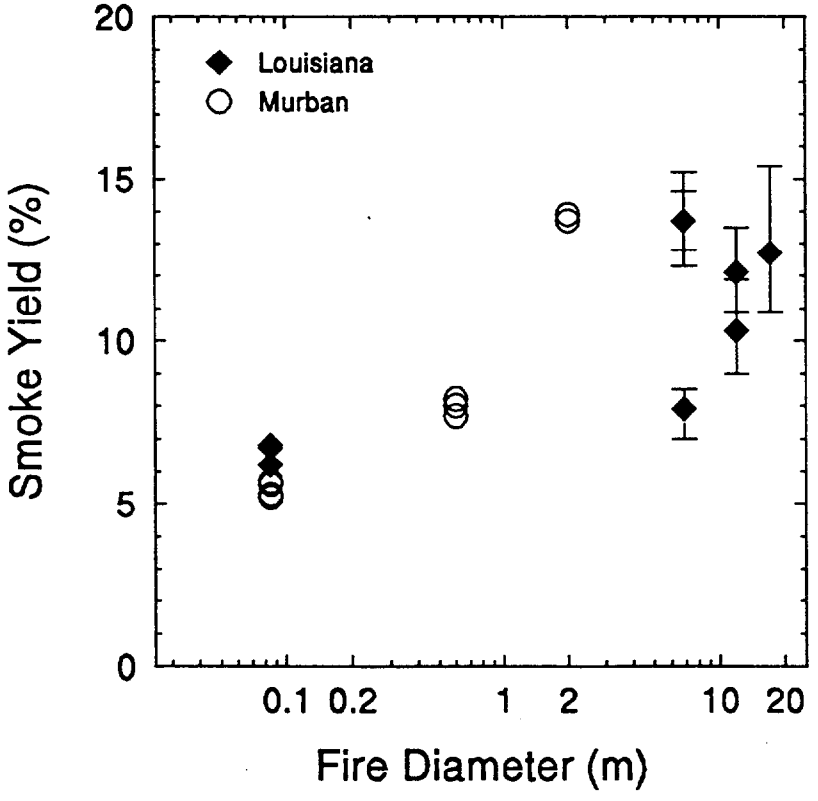

Figure 8. Smoke yield by carbon balance method (all scales)

Table 14. Smoke yield from mesoscale burns

Mesoscale Burn No.	Effective Diameter (m)	Smoke Yield	Uncertainty Interval
4/6/91	6.88	0.137	0.123 - 0.152
5/17/91	6.88	0.079	0.070 - 0.085
5/22/91 Water spray	12.0	0.103	0.090 - 0.119
5/29/91 Aged Oil	6.88	0.137	0.128 - 0.146
6/3/91	12.0	0.121	0.109 - 0.135
6/5/91	17.2	0.127	0.109 - 0.154

PARTICLE SIZE DISTRIBUTION

Particulate size is an important health consideration and also impacts the dynamics of smoke settling. Particulates having an aerodynamic effective diameter less than 10 μm are considered respirable [16] and may be drawn into the lungs with normal breathing. In general small particle sizes have the greatest resistance to settling and can be expected to be carried much further from the burn site than larger particles. In addition to the overall particulate yield from the crude oil fires, it is therefore important to have some knowledge about the particulate size distribution. Smoke particles are an agglomeration of individual spherules. Figure 9 shows a tunneling electron micrograph of smoke particulate emitted from a 1 m diameter crude oil fire. The spherules that make up the structure of the smoke particulate are relatively uniform in size with an average diameter of 0.06 μm. Measurements of smoke particles from 3 m diameter crude oil fires have shown a mixture of spherule diameters in two groupings of 0.15 and 0.06 μm [11].

There is no means to directly translate the observed irregular shape of smoke particles into aerodynamic effective diameters. The aerodynamic effective diameter of a particle is defined as the diameter of a smooth spherical particle with a unit density of 1000 kg/m^3 (1 g/cm^3) that has the same settling velocity in air. Therefore, the aerodynamic effective diameter of a particle depends on the size, shape and density of the particle. Cascade impactors measure particle size distribution by the amount of particulate deposited on a series of plates. The particulate laden air is drawn through the cascade impactor which consists of a series of stages each having a nozzle and plate. Aerodynamic forces determine the size ranges that will be deposited on the plate in each stage and the sizes that will pass through to other stages down-stream. The fraction of the total deposition collected by each stage of the device

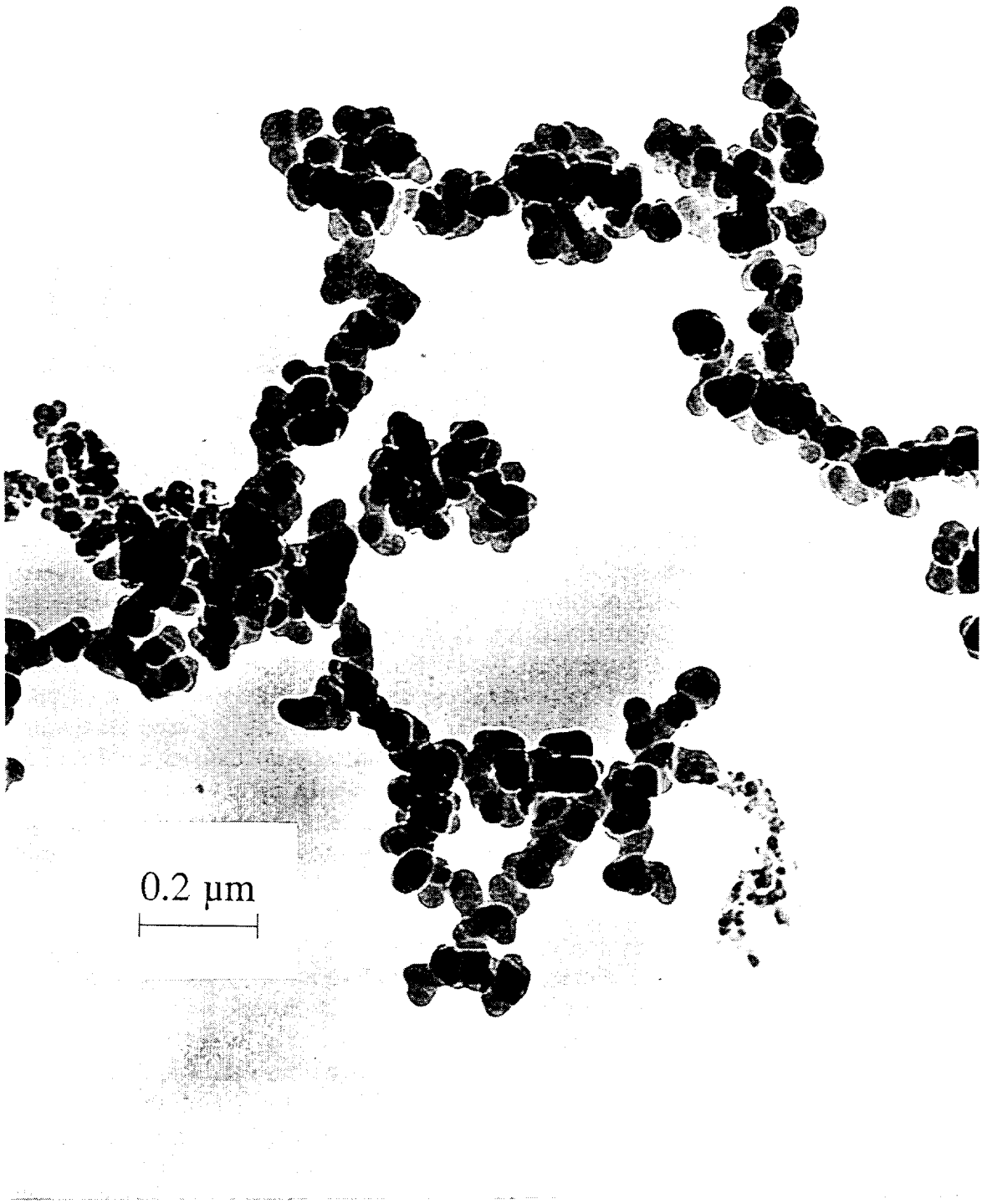

Figure 9. **Electron micrograph of a smoke particle from a 1.0 m diameter Murban crude oil fire**

determines the distribution of the aerodynamic effective diameter of the particles. The small and light weight commercial impactors used in this study contained six stages. For cases where a small quantity of particulate is expected, some of the stages may be removed. The cutpoint diameter is the aerodynamic effective diameter that is collected with 50 percent efficiency. Ideally the cutpoint diameter represents the largest diameter particle which will not pass to the next stage but in practice some larger particles do move to the next stage. The cut point diameter is a function of the flow rate through the instrument and decreases with increasing flow rate.

In the mesoscale experiments, the impactor was operated at a flow rate of 0.054 L/s with four stages to assure sufficient particulate deposition in each stage. In the laboratory experiments, the impactor was operated at the manufacturers recommended flow rate of 0.033 L/s and all six stages were used. The cutpoint diameters for each stage were determined using the standard correction methods for the instrument [17]. Table 15 shows the cutpoint diameters for each of the stages in the instrument and the back-up filter at the two flow rates used in this study.

Figure 10 shown the cumulative size distribution of smoke particulate from a 2.0 m diameter Murban crude oil fire in the laboratory and a 12.0 m effective diameter Louisiana crude oil mesoscale fire. A comparison of the results from the two fires shows that there is a greater number of smaller particles in the 2.0 m diameter fires than in the 12.0 m diameter fires. For the 2.0 m diameter fires 71% of the particles have an aerodynamic effective diameter of 0.52 μm or less while for the 12.0 m diameter fires 13% have an effective diameter of 0.39 μm or less. For the 2.0 m diameter fires 1% of the particles have an effective diameter of 9.8 μm or greater while for the 12.0 m diameter fires 16 % have a diameter of 7.8 μm or greater.

Table 15. Cascade impactor stage cutpoint size diameters

Flow Rate (L/s)	Stage 1 μm	Stage 2 μm	Stage 3 μm	Stage 4 μm	Stage 5 μm	Stage 6 μm	Back-up Filter μm
0.033	9.8	6.0	3.5	1.55	0.93	0.52	0
0.054	7.8	---	---	1.2	0.70	0.39	0

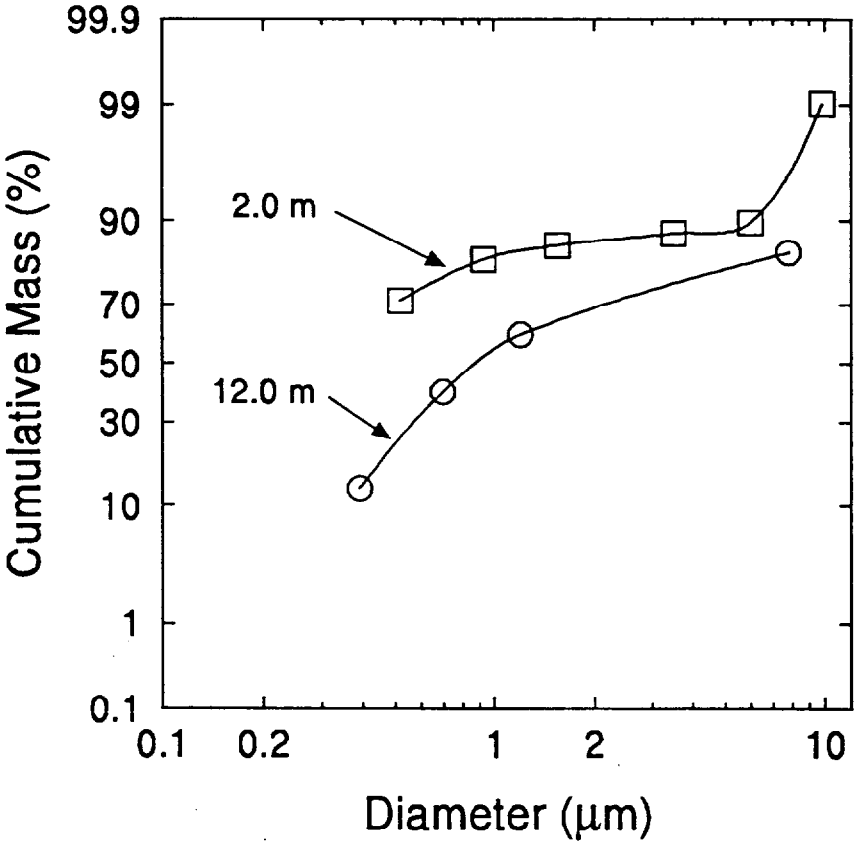

Figure 10. **Size distribution of smoke particulate from a 2.0 m diameter Murban crude oil fire and a 12.0 m diameter Louisiana crude oil fire**

FIRE PULSATIONS

A natural phenomenon associated with all buoyant diffusion flames is the regular pulsation of the flame caused by interactions with air flow near the base of the flame. For small fires this "flicker" of the flame is well known. Larger laboratory fires also have regular pulsations that generate large scale structures in the smoke plume flow. The frequency of these pulsations (vortex shedding frequency) has been correlated for fire diameters from 0.03 m to 50 m by the equation [18]:

$$f = 1.5 / \sqrt{D} \qquad (4)$$

where:

f = pulsation frequency (Hz)
D = effective diameter of the fire (m)

This correlation shows there is a strong decrease in the frequency of the pulsations with increasing diameter of the fire. In measurements using a gas burner, Hamins [19] has shown that the pulsation frequency of flames was not sensitive to a factor of two variation in heat release rate with a constant exit velocity of the fuel, although wind is thought to lead to substantial changes in the pulsation frequency [20].

Table 16. Pulsation frequency of pool fires

Burn	Effective Diameter (m)	Wind Speed (m/s)	Frequency Before Boiling (Hz)	Frequency During Boiling (Hz)	Predicted Frequency Eqn. (4) (Hz)
Mesoscale					
5/17	6.88	1.7	0.73±0.08	---	0.57
5/29	6.88	5.0	0.70±0.04	---	0.57
6/3	12.0	1.0	0.42±0.03	0.56±0.07	0.43
6/4	12.0	2.1	0.42±0.07	0.45±0.05	0.43
5/31	17.2	0.8	0.46±0.04	0.44±0.04	0.36
FRI, Japan					
	2.0	---	1.13±0.05	1.29±0.08	1.1

Video recordings of the mesoscale experiments, and 2 m diameter crude oil fires experiments at FRI were analyzed to determine the pulsation frequency of the fire by observing the motion of the flame near the fuel surface. Table 16 lists the measured values of pulsation frequency along with effective fire diameter for the mesoscale experiments and the pan burns at FRI in Japan. For the mesoscale experiments the

near surface wind speed is also listed. For some of the mesoscale fires, a pulsation frequency before and after the onset of boiling was measured. In two of the three experiments in which the burning continued for sufficient time after the onset of boiling to measure the pulsation frequency, no significant increase was found. For the smallest mesoscale experiments (effective diameter of 6.88 m) an increase of almost a factor of three in wind speed did not significantly change the pulsation frequency of the fire. Measurements are generally in agreement with predictions using equation (4) and the data from other fires given in reference [18]. The largest variation, about 1/3 of the predicted frequency, occurred for the 17.2 m effective diameter burn.

SMOKE PLUME TRAJECTORY MEASUREMENTS

Although there are many accidental fires that produce smoke plumes, these opportunities are not useful for gathering data that is needed to validate predictive methods for smoke plume trajectory and particulate deposition. This is because the smoke production and heat release rates of the fire are unknown. The mesoscale pan fire experiments provided a unique opportunity to measure smoke plume trajectories for burns of known particulate emission and fuel burning rates. Measurements of smoke plume trajectories were made in half of the mesoscale burns. The trajectory and radius of the smoke plume were measured using video recordings and subsequently analyzed using digital image processing. Results of these measurements and discussion of the data reduction techniques have been reported by Leonard, et al. [21].

Ideally, measurement of smoke plume trajectory and cross section would be performed using a combination of near field ground observations and long-range measurement from an aircraft following the plume downwind. Near-field ground based measurements were used in this study to measure the initial plume trajectory and cross section over a distance of 1 to 2 km from the source. Both video and still photography images of the initial rise of the smoke plume from the pan were recorded. Distances on these images were scaled from known distances between fixed objects in the field of view.

Since it was not always practical to view the smoke plume perpendicular to the direction of flow, adjustments for oblique viewing angles were made during the data analysis. Figure 11 shows the geometric correction to the observed plume length from a camera at an oblique angle to the wind-blown plume direction. The true plume length (a') is calculated from the observed length (a) as:

$$a' = a/\sin\beta \tag{5}$$

where β is the angle between the nominally crosswind camera view and the smoke plume centerline direction.

The plume radius as a function of distance from the source was measured as part of the analysis. At selected segments of the plume (see figure 12), the radius of the plume was determined at seven locations equidistant along the plume centerline. The

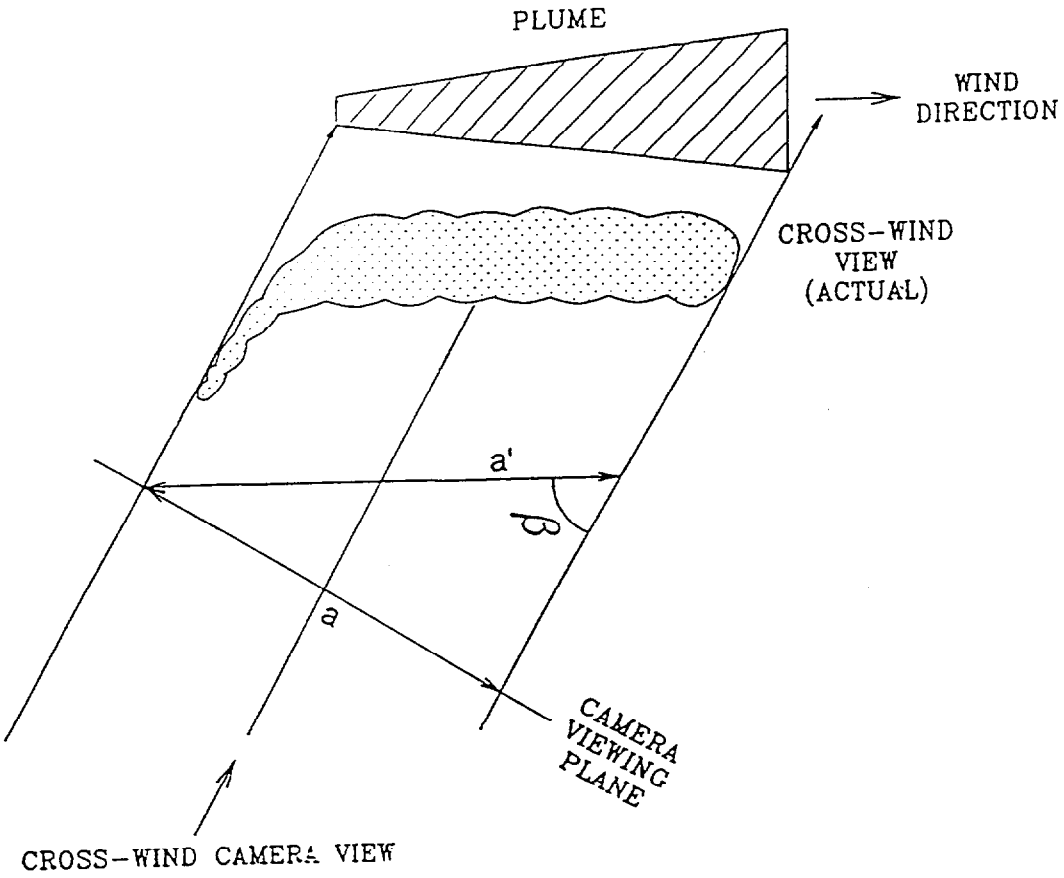

Figure 11. Geometric correction for plume length when observed from an oblique angle

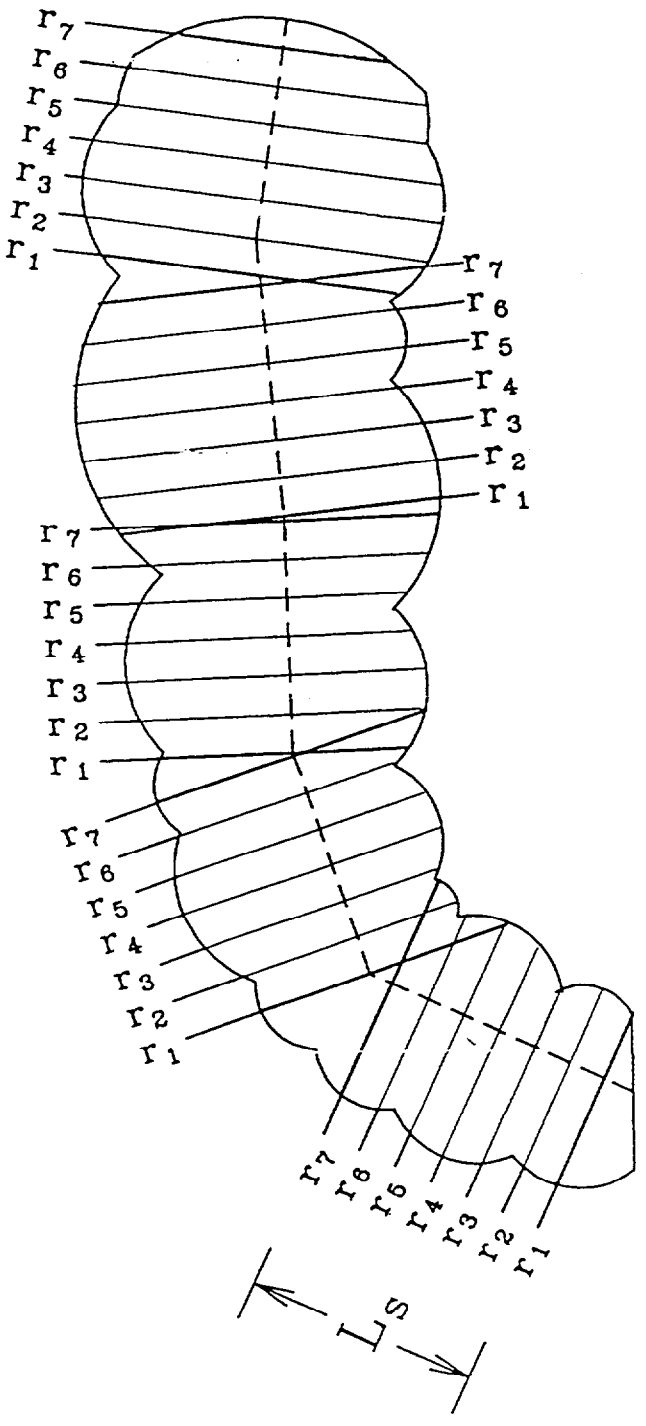

Figure 12. Segments used to calculate plume volume

highest and lowest values were ignored, and the remaining five values were averaged as the best estimate for the radius of that segment. Each segment can be approximated as a cylinder with radius equal to the average radius of the segment, and length equal to the length of the segment. The volumes of the segments can be added together over the entire length of the plume to estimate the total plume volume as:

$$V_p = \sum_{n=1}^{N} \pi r_n^2 l_n \qquad (6)$$

where V_p = Volume of the plume
n = Segment number
N = Total number of segments
r = radius of a cylindrical segment
l = length of a cylindrical segment

Of the experiments in which measurements were made, mesoscale burn 5/30 provided data on plume trajectory for the largest distance from the pan. As listed in table 5, for this burn the wind direction was from the south-south-east at 170 degrees from magnetic north. The nominal wind speed was 3 m/s at 2 m above ground and 6.2 m/s at 48 m above ground. The crosswind camera recording the plume images was located 3500 m from the pan to the north-east, 70 degrees from magnetic north (across Mobile Bay). Therefore, the crosswind camera was nearly perpendicular to the plume direction. The angle (β) between the camera viewing direction and the plume was 80 degrees. Figure 13 shows a sequence of plume photographs taken from the crosswind camera and the corresponding digitized images at one minute intervals for the first five minutes after ignition. This shows good agreement between the visual plume and the images used for digital analysis. Figure 14 shows digitized images of the plume used for volume and trajectory analysis over the first 600 s after ignition.

Table 17. Initial smoke plume characteristics for mesoscale burn 5/30

Elapse Time (s)	Height (m)	Distance (m)	Volume (m^3 x 10^6)	Volume Rate of Change (m^3/s x 10^6)
120	160	430	1.8	0.015
240	380	730	10.4	0.072
360	480	1130	58	0.39
480	660	1350	130	1.1
600	780	1820	380	3.2

Table 17 summarizes the results for plume rise, plume volume, and rate increase in plume volume. Measured plume rise heights for the first 600 s after ignition are

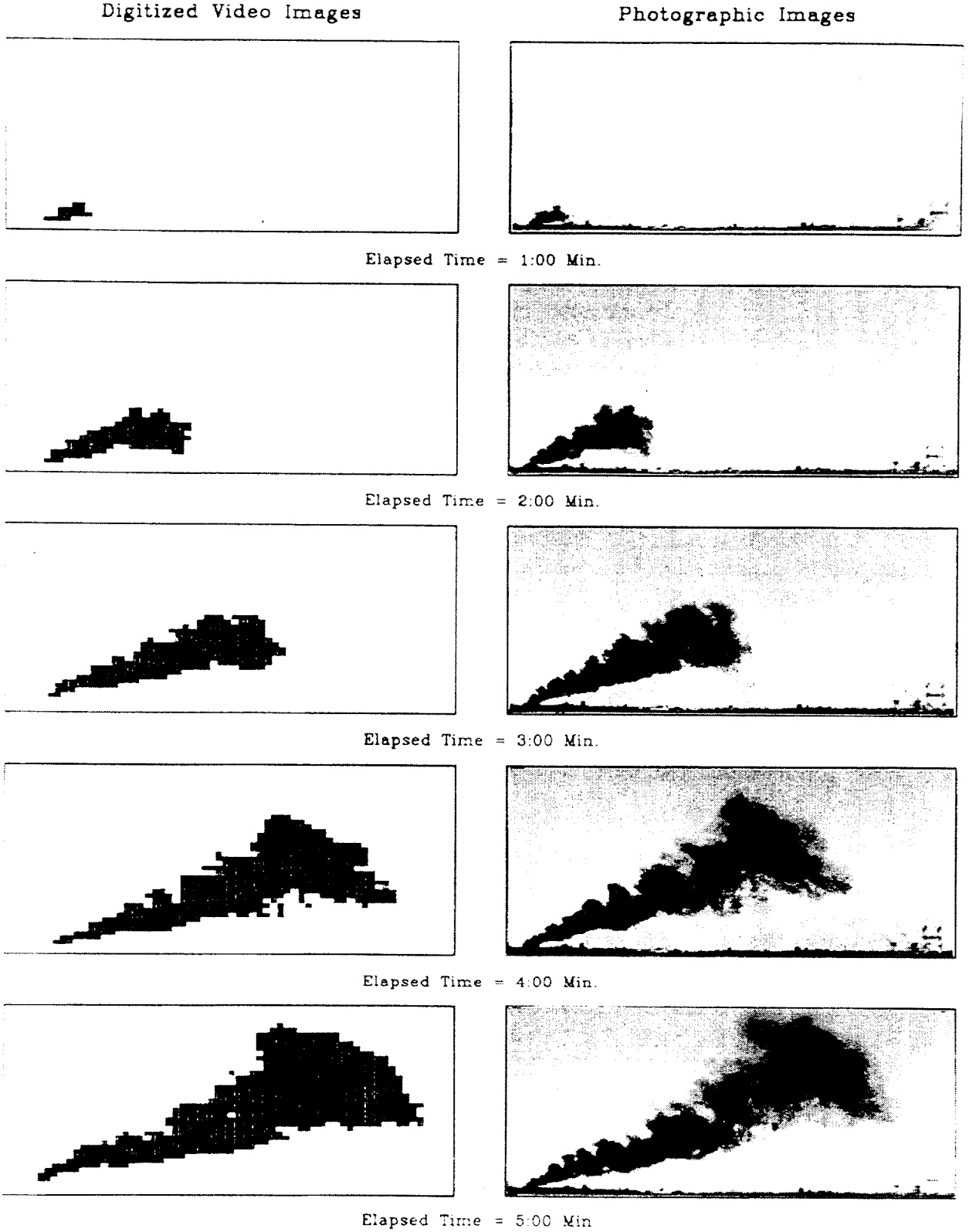

Figure 13. Plume photographs and corresponding digitized images for mesoscale burn 5/30

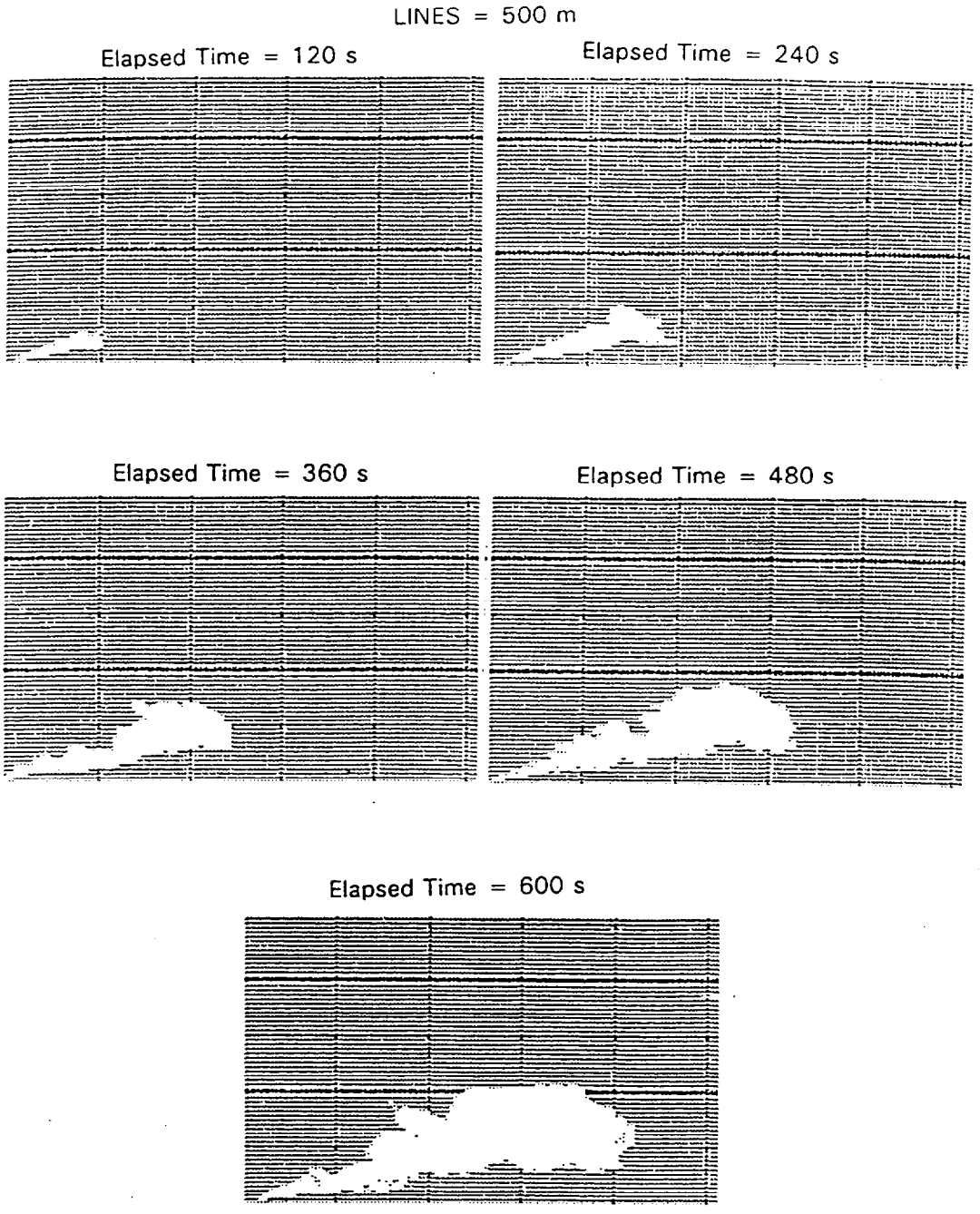

Figure 14. Digital images used in analysis of mesoscale burn 5/30

plotted in figure 15. At 600 s after ignition the leading edge of the smoke plume had risen to 780 m and traveled 1800 m downwind from the pan. The estimated total volume of the plume at 600 s after ignition was 3.8 x 10^8 m^3. At that time, the total volume of the smoke plume was increasing at a rate of 3.2 x 10^6 m^3/s. This rate of volume increase is largely the result of mixing of smoke particulate in the plume with surrounding air as opposed to the injection of newly formed smoke particulate from the burning crude oil. Table 18 lists the radii of the plume for various downwind distances as determine from analysis of the digitized image of the plume 10 minutes after ignition. These data show the expansion of the smoke plume depth from 40 m near the source to 820 m near the leading edge, 1820 m downwind from the source.

Table 18. Height and radii of the smoke plume 10 minutes after ignition for mesoscale burn 5/30

Downwind Distance (m)	Centerline Height (m)	Effective Diameter (m)
0	0	0
110	40	40
210	80	130
320	120	230
430	160	320
540	200	420
640	240	400
750	310	610
860	380	540
970	440	460
1070	510	480
1180	580	550
1290	640	640
1390	670	730
1500	700	820
1610	730	780
1720	750	720
1820	780	820

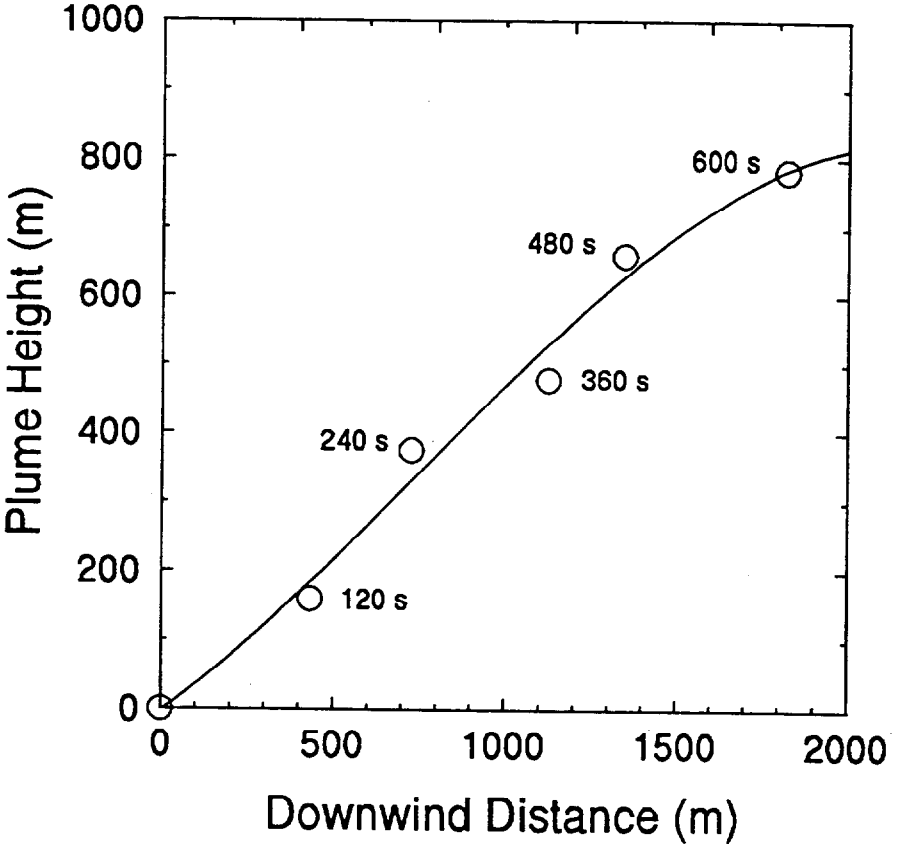

Figure 15. Plume height vs downwind distance for mesoscale burn 5/30

SMOKE PLUME TRAJECTORY MODELING -- LES MODEL

A principal concern in the decision to use in-situ burning as an oil spill mitigation technique is the anticipated trajectory of the plume and the settling out of particulates. The smoke plume trajectory model presented earlier [11] has been generalized to include the capability to describe the rising thermally dominated portion of the smoke plume as well as the descent of the cool, negatively buoyant smoke. A simplified description of the mean thermal stratification of the atmosphere is also included. The wind in the undisturbed atmosphere is still assumed to be uniform on average, but the small scale random eddy motion induced by the natural turbulence in the atmosphere is now represented by an effective "eddy viscosity". A computer code based on an existing enclosure fire simulation program [22] has been developed to implement the model. The resulting code, called LES for Large Eddy Simulation, can be readily generalized to include realistic time averaged ambient temperature and wind profiles in the atmosphere. A summary of the basic assumptions built into the current version of the LES code are given below. This is followed by a summary of the mathematical model which follows from these assumptions. Finally, results showing the full plume trajectory as well as the particulate deposition footprint on the ground as predicted by the model are shown. Comparisons with data obtained in the mesoscale burns are made where appropriate.

We assume that the plume may be described in terms of the steady state physical location of the heated gas and particulate matter introduced by the continuously burning fire into the atmosphere. For this purpose it is not necessary to describe the fire in detail, provided that the overall rate of heat release and the fraction of the fuel converted to particulate matter are known, and the initial plume structure within a few flame lengths of the firebed is not of interest. The subsequent location of the plume as it is carried downwind is determined by the ambient wind and density profiles in the atmosphere along the trajectory of the plume. Since it is not our objective to calculate the local meteorology, it is assumed that this information is available as well. At present, the model is only able to incorporate a uniform wind and a temperature decreasing linearly with height above ground level. The magnitude of both the temperature rise in the plume and the induced velocity fields are assumed to be small compared to their mean values in the undisturbed atmosphere. Finally, the atmosphere is turbulent even in the absence of the fire. This affects the mixing on scales smaller than the resolution of the calculations performed here. The consequences of the small-scale mixing are represented by a constant eddy viscosity, which is ultimately determined by the turbulent kinetic energy content of the atmosphere at "subgrid" scales. This information must be inferred from either measurements of the undisturbed atmosphere or the plume trajectory.

LES MATHEMATICAL MODEL

Given the assumptions outlined above, the mathematical model of the smoke plume requires a description of the gas temperature T and pressure P, the particulate density ρ_p, and the horizontal (y) and vertical (z) velocity components (v,w) in a plane normal

to the direction (x) of the ambient wind U. It is convenient to divide the temperature and pressure fields into mean background values $T_o(z)$ and $P_o(z)$ respectively plus perturbations to these quantities induced by the plume. Let θ and p be the small perturbations to the temperature and pressure respectively. Similarly, the gas density ρ_g is decomposed into an ambient density ρ_o and a small thermally induced perturbation. This perturbation is related to the temperature perturbation through the equation of state which is taken in the small disturbance low Mach number form appropriate to this problem:

$$(\rho_g - \rho_o)/\rho_o = - (T - T_o)/T_o \tag{7}$$

The ambient density is related to the background pressure through the hydrostatic balance :

$$\frac{dP_o}{dz} = - \rho_o g \tag{8}$$

The background temperature is taken to be linearly stratified:

$$T_o(z) = T_\infty (1 - z/H) \tag{9}$$

Here, T_∞ is the ground level temperature and H is a length of order 10 km. Thus, over the first 1 or 2 km in altitude, the background temperature changes by only a small fraction of its value at ground level. This, together with equation (8), ensures that the fractional variation of the absolute temperature and density are small if the plume calculation begins a few flame lengths downwind of the firebed. Under these circumstances the equations governing the steady-state downwind evolution of the plume can be written in the Boussinesq approximation as follows:

Conservation of mass

$$\frac{\partial v}{\partial y} + \frac{\partial w}{\partial z} = 0 \tag{10}$$

Conservation of lateral (y) momentum

$$\rho_o\left(\frac{U\partial v}{\partial x}+\frac{v\partial v}{\partial y}+\frac{w\partial v}{\partial z}\right)+\frac{\partial p}{\partial y}=\mu\left(\frac{\partial^2 v}{\partial y^2}+\frac{\partial^2 v}{\partial z^2}\right) \tag{11}$$

Conservation of vertical (z) momentum

$$\rho_o\left(\frac{U\partial w}{\partial x}+\frac{v\partial w}{\partial y}+\frac{w\partial w}{\partial z}\right)+\frac{\partial p}{\partial z}+(\rho-\rho_o)g=\mu\left(\frac{\partial^2 w}{\partial y^2}+\frac{\partial^2 w}{\partial z^2}\right) \tag{12}$$

Conservation of energy

$$\rho_o C_p\left(\frac{U\partial\theta}{\partial x}+\frac{v\partial\theta}{\partial y}+\frac{w\partial\theta}{\partial z}\right)-\left(\frac{dP_o}{dz}+\frac{\rho_o C_p T_\infty}{H}\right)w=k\left(\frac{\partial^2\theta}{\partial y^2}+\frac{\partial^2\theta}{\partial z^2}\right) \tag{13}$$

Conservation of particulate mass

$$\frac{U\partial\rho_p}{\partial x}+\frac{v\partial\rho_p}{\partial y}+\frac{w\partial\rho_p}{\partial z}=0 \tag{14}$$

The windward component of the velocity U in these equations is taken to be constant and much larger than the velocity components in the lateral and vertical directions. Since U does not change, there is no need for a windward component of the momentum equations. After the first few flame lengths downwind of the firebed, the assumption that the windward component of the velocity is much larger than that induced by the plume is quite realistic.

The quantity μ denotes the effective eddy viscosity in the undisturbed atmosphere. It is used here as a means to represent the small scale mixing induced by the atmospheric turbulence. The eddy viscosity is dependent on the level of turbulence in the atmosphere, and is typically about three orders of magnitude larger than the true molecular viscosity of the air. Note that we are only using this concept to simulate the "subgrid" scale motions; i.e. motions on scales below the 5-10 m range which is the resolution limit for the calculations reported here. The large scale mixing processes, from length scales of 1-2 km down to the resolution limit, are calculated directly. Thus, even with the assumption of an eddy viscosity model for the small scale turbulence, the "large eddy" simulations performed require an ability to simulate flows at quite high Reynolds numbers.

In order to complete the mathematical formulation of the problem, initial and boundary conditions must be specified. Since the details of the firebed are not being simulated, the only quantities that are retained are the overall "conserved" parameters,

the total heat release rate Q and the particulate mass flux M. They are related to the local field variables introduced earlier as follows:

$$\int_{-\infty}^{\infty} dy \int_{o}^{\infty} dz \; \rho_o C_p \, \theta U = Q$$

$$\int_{-\infty}^{\infty} dy \int_{o}^{\infty} dz \; \rho_p U = M \tag{15}$$

These quantities do not change as the plume moves downwind from the firebed in the absence of ambient stratification in the atmosphere. Thus, these quantities are preserved for the first several pool diameters downwind and can be specified with consistently chosen temperature and particle density crosswind profiles as the initial conditions for the plume temperature θ and particle density ρ_p. The crosswind velocity components v and w are assumed to be zero initially. This ensures that the velocities in the crosswind plane are induced only by the buoyancy in the plume. The boundary conditions at ground level assume no vertical velocity and no plume induced heat transfer or wind shear at ground level. These assumptions are consistent with the assumed uniformity of the ambient wind and the resolution limits imposed by the available computational resources. They are expressed in mathematical form as:

$$w = \frac{\partial v}{\partial z} = \frac{\partial \theta}{\partial z} = 0 \quad at \; z = 0 \tag{16}$$

Finally, the far field conditions in the crosswind plane require that the perturbation temperature vanish and the windward component of the vorticity induced by the plume vanish as y and z approach the edge of the computational domain. The perturbation pressure p at the edge of the computational domain can be determined in a self-consistent way by calculating it from the solution of a Poisson equation obtained by requiring that equation (10) holds everywhere. As a practical matter, however, the difference between applying the boundary condition obtained in this way and simply requiring p to vanish at the computational boundary is negligible in the computations performed to date. Hence, the far field boundary conditions implemented in the present model are:

$$\frac{\partial w}{\partial y} - \frac{\partial v}{\partial z} = \theta = p = 0; \; y,z \rightarrow \infty \tag{17}$$

Note that no boundary conditions are explicitly specified for the particulate density ρ_p. This is due to the fact that equation (14) implies that the particles are advected by the large eddy flow field. Hence, once they are introduced into the flow as part of the initial conditions, no further specification is required or possible. In reality however, when the particulate matter reaches the vicinity of the ground,it settles out and is lost from the atmosphere. This is accounted for in the present model by calculating the particulate density as a large number of discrete parcels (Lagrangian

elements) that are carried about by the fluid. Any element that arrives within one computational cell of the ground is within the resolution limits of the calculation of having settled out of the atmosphere. It is then removed from the computation and the location where it settled out of the atmosphere recorded. In this way the "footprint", the distribution on the ground of the particulate matter that has settled out of the atmosphere, can be calculated.

Since the computations that must be performed to solve these equations are quite large, the equations are made nondimensional so that the maximum amount of information can be extracted from each run. The dependent and independent variables are scaled as follows:

$$
\begin{gathered}
\theta/T_\infty = (Q/C_pT_\infty\rho_oUL^2)\ \hat{\theta}\ (\hat{t},\hat{y},\hat{z}) \\
\rho_p/\rho_o = (M/\rho_oUL^2)\ \hat{\rho}_p\ ;\ p = \rho_oV^2\hat{p} \\
(v,w) = V\ (\hat{v},\hat{w})\ ;\ V = (Qg/C_pT_\infty\rho_oUL)^{1/2} \\
X = (UL/V)\ \hat{t}\ ;\ L = (QH/C_pT_\infty\rho_oU\beta)^{1/3} \\
\beta = \left(\frac{(\gamma-1)gH}{C_o^2} - 1\right);\ C_o^2 = \gamma RT_\infty \\
(y,z) = L\ (\hat{y},\hat{z}) \\
R_e = \rho_oVL/\mu\ ;\ P_r = \mu C_p/k
\end{gathered}
\tag{18}
$$

The length scale L introduced in equation (18) replaces the arbitrary length used to describe the initial extent of the descending particle plume in [11]. Physically, it is a measure of the height at which the thermal plume will equilibrate with the atmosphere. Note that it depends upon the stability of the atmosphere which is measured by the value of the parameter β. When β is positive, the atmosphere is stable and the plume will reach a maximum height of order L. If β is not positive, the lower atmosphere is not stable and the plume will rise to high altitudes and its fate will be determined by the large scale regional and national weather patterns. In that case the model cannot predict the subsequent deposition pattern of the particulate matter. Note also that the plume model also relies for its validity upon the assumption that the velocity V used to scale the crosswind components of the velocity field in equation (18) is much smaller than the windward velocity component U. This seems to be true for the calculations performed to date.

The dimensionless form of the conservation laws are:

$$\frac{\partial \hat{v}}{\partial \hat{y}} + \frac{\partial \hat{w}}{\partial \hat{z}} = 0$$

$$\frac{\partial \hat{v}}{\partial \hat{t}} + \hat{v}\frac{\partial \hat{v}}{\partial \hat{y}} + \hat{w}\frac{\partial \hat{v}}{\partial \hat{z}} + \frac{\partial \hat{p}}{\partial \hat{y}} = \frac{1}{R_e}\left(\frac{\partial^2 \hat{v}}{\partial \hat{y}^2} + \frac{\partial^2 \hat{v}}{\partial \hat{z}^2}\right)$$

$$\frac{\partial \hat{w}}{\partial \hat{t}} + \hat{v}\frac{\partial \hat{w}}{\partial \hat{y}} + \hat{w}\frac{\partial \hat{w}}{\partial \hat{z}} + \frac{\partial \hat{p}}{\partial \hat{z}} + \frac{\hat{\rho}}{\alpha} - \hat{\theta} = \frac{1}{R_e}\left(\frac{\partial^2 \hat{w}}{\partial \hat{y}^2} + \frac{\partial^2 \hat{w}}{\partial \hat{z}^2}\right) \qquad (19)$$

$$\frac{\partial \hat{\theta}}{\partial \hat{t}} + \hat{v}\frac{\partial \hat{\theta}}{\partial \hat{y}} + \hat{w}\frac{\partial \hat{\theta}}{\partial \hat{z}} + \hat{w} = \frac{1}{P_r R_e}\left(\frac{\partial^2 \hat{\theta}}{\partial \hat{y}^2} + \frac{\partial^2 \hat{\theta}}{\partial \hat{z}^2}\right)$$

$$\frac{\partial \hat{\rho}_p}{\partial \hat{t}} + \hat{v}\frac{\partial \hat{\rho}_p}{\partial \hat{y}} + \hat{w}\frac{\partial \hat{\rho}_p}{\partial \hat{z}} = 0$$

Finally, the associated initial and boundary conditions take the form:

$$\hat{\rho}_p = \hat{\rho}_I(\hat{y},\hat{z}) \; ; \; \hat{\theta} = \hat{\theta}_I(\hat{y},\hat{z}) \; ; \; \hat{v} = \hat{w} = 0 \quad at \; \hat{t} = 0$$

$$\int\int d\hat{y}d\hat{z}\hat{\rho}_I(\hat{y},\hat{z}) = 1 \; ; \; MC_pT_\infty/Q \equiv 1/\alpha$$

$$\int\int d\hat{y}d\hat{z}\hat{\theta}_I(\hat{y},\hat{z}) = 1 \qquad (20)$$

$$\hat{w} = \frac{\partial \hat{v}}{\partial \hat{z}} = \frac{\partial \hat{\theta}}{\partial \hat{z}} = 0 \quad at \; z = 0$$

$$\frac{\partial \hat{w}}{\partial \hat{y}} - \frac{\partial \hat{v}}{\partial \hat{z}} = \hat{p} = \hat{\theta} = 0 \; ; \; \hat{y},\hat{z} \to \infty$$

Note that in these variables the conservation laws depend only upon the Reynolds and Prandtl numbers, which characterize the ratio of the relative effectiveness of the large scale transport to the small scale mixing in the atmosphere, and upon the ratio $Q/(MC_pT_\infty)$, which characterizes the ratio of the positive thermal buoyancy to the negative particulate buoyancy. The details of the initial crosswind profiles serve only to characterize the overall dimensions of the firebed, and are quickly washed out as the plume mixes with the atmosphere.

LES COMPUTED RESULTS

The equations and boundary conditions described above are solved in the LES using finite difference techniques described in [22]. The computational domain is taken to be one unit (in L) high and two units in width. It is divided into a rectangular grid 256 cells high and 512 cells wide for the calculations described below. The Reynolds number employed in the simulation is 20,000, which is within the resolution limits of the grid. The calculation proceeds downwind a distance of 15 units in UL/V, which is enough to ensure that at least 90 percent of the particulate matter injected into the atmosphere in the simulation has settled out. The number of downwind steps required to carry out the computation cannot be prescribed a priori, but is determined

by the numerical stability requirements of the underlying algorithm. For the calculations described below, a minimum of about 6000 steps is required. The particulate matter is represented by 6000 discrete Lagrangian elements which are carried about by the combination of atmospheric and buoyancy induced winds. The particles are not passive; indeed it is their collective negative buoyancy which ultimately causes them to settle out of the atmosphere. They are injected randomly in the vicinity of the firebed with zero initial velocity, and tracked until they reach a computational cell near the ground where they are removed. This final distribution of the locations of the removed particles is the footprint.

The computations have been carried out on an IBM RISC System 6000 model 550.[1] Using a grid of the size described above, the calculations require about 5 seconds to complete a step in the downwind direction. Approximately 30 megabytes of memory are required to accommodate the entire calculation and the associated output buffers. It should be noted that this is less than half the available memory on the minimum available configuration of this particular computer. In fact, the mathematical model and the associated LES have been developed with the idea that they can be used on a variety of high performance workstations available from several computer manufacturers.

Figures 16 and 17 illustrate results obtained from a simulation using data from mesoscale burn 5/30. The burn generated an estimated 0.5 kg/s soot particulate mass flux in a fire whose convective heat release rate is estimated at 110 MW. The wind velocity was measured at 6 m/s. The computational domain is then 1.6 km high, 3.2 km wide, and 258 km in the downwind direction.

Figure 16 shows the locations of the particle plume at eleven stations downwind of the fire extending out the first 190 km downwind from the fire. The plume is initially dominated by the large heat input from the fire and the plume rises rapidly to a maximum height of about 0.8 km. The smoke plume gradually separates from the thermal plume, however, once the stabilized height is reached. This is due to a combination of small scale mixing processes and the stratification of the atmosphere. After the separation of the thermal and particle plumes, the negatively buoyant particle plume gradually descends to the ground. Near ground level the lateral spreading is enhanced by the interaction of the vorticity in the plume with the ground plane. Finally, in the final 6.25 m (the size of one computational cell) the particulate matter is assumed to settle out of the atmosphere and is removed from the computation. The reader is reminded to note the difference in downwind and crosswind scales in figure 16; even with the enhanced spreading near the ground the plume is a long, slender object.

Figure 17 shows the computed footprint in the ground plane out to 258 km, where over ninety percent of the particulate matter has settled out of the plume. The particles are distributed in long striations which are caused by the ground induced vortex motion which produces highly organized motion near the surface. This plot indicates that the density distribution on the ground is far from uniform, so that the average value of 1.5 mg/m^2 over the whole footprint is not a reliable indicator of the

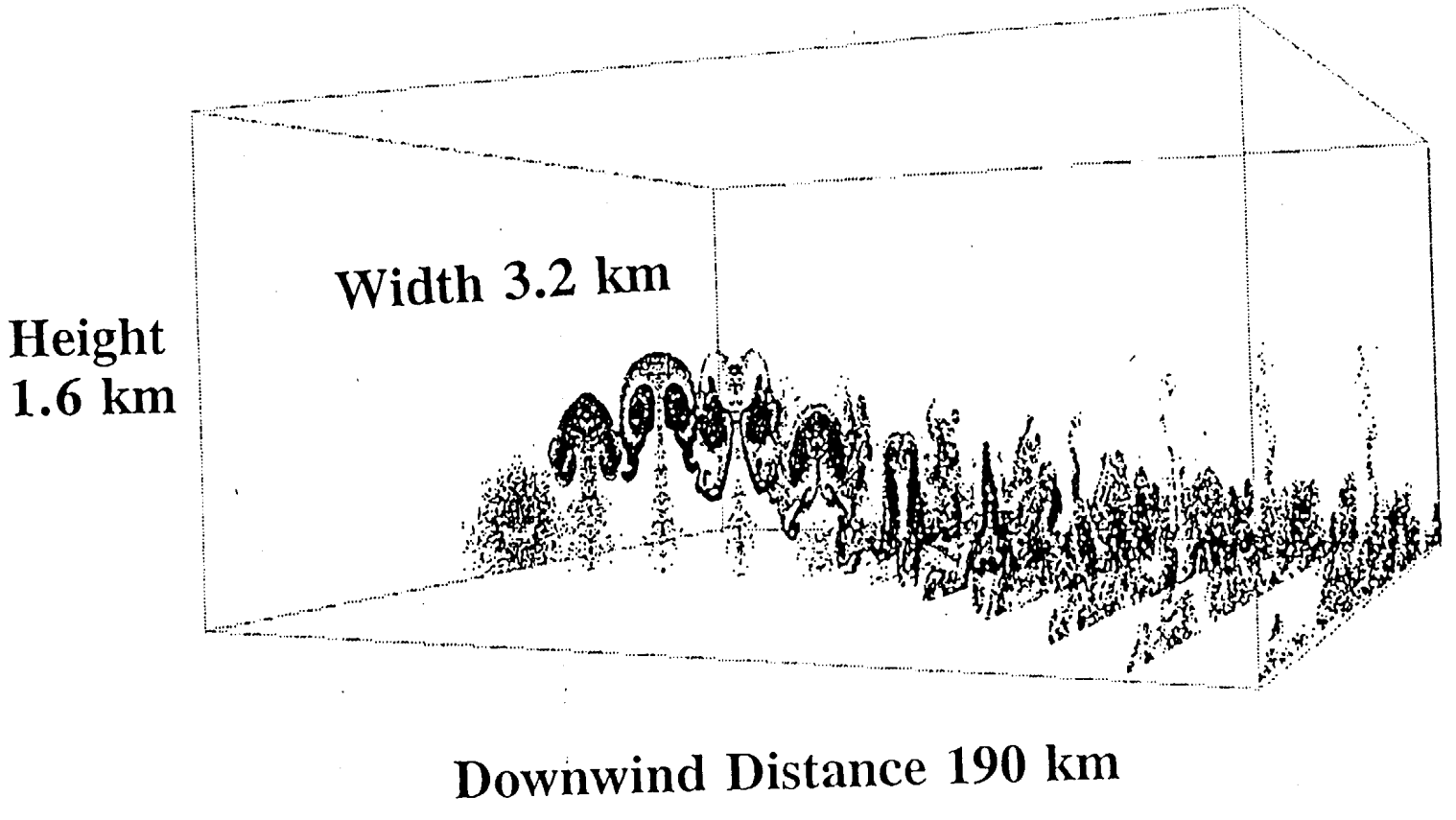

Figure 16. LES prediction of downwind particulate distribution in the air

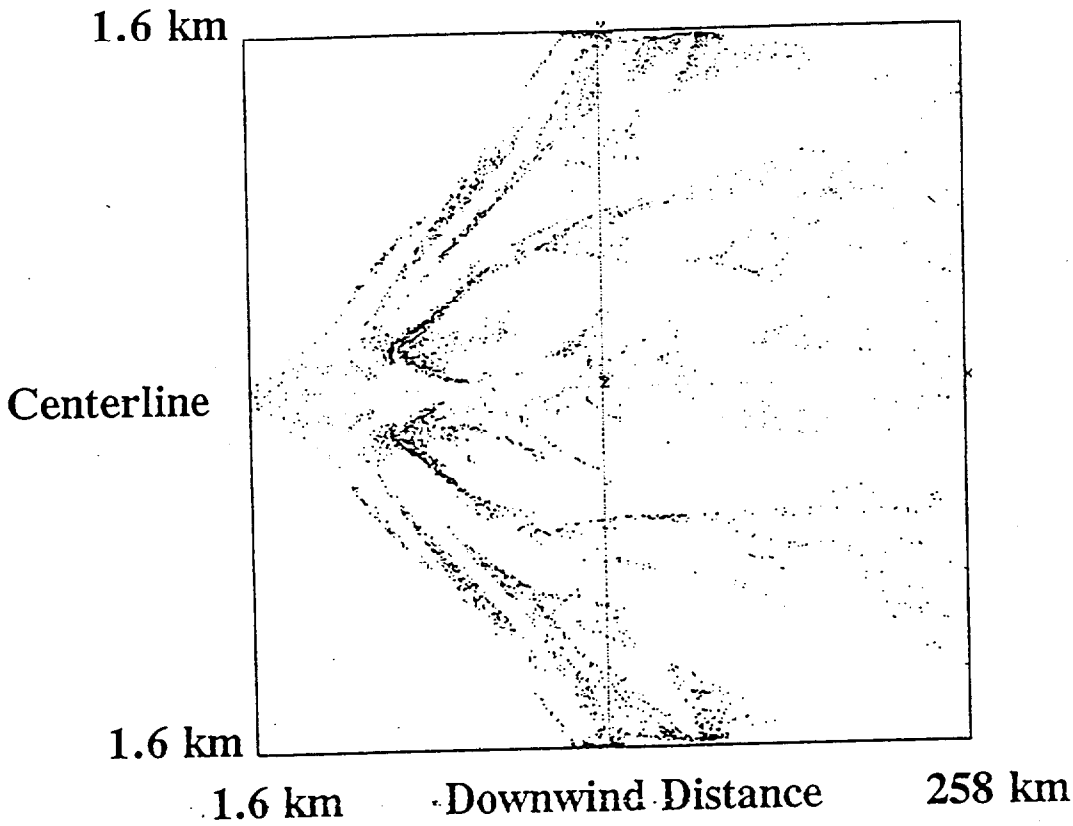

Figure 17. LES prediction of the pattern of downwind particulate deposition.

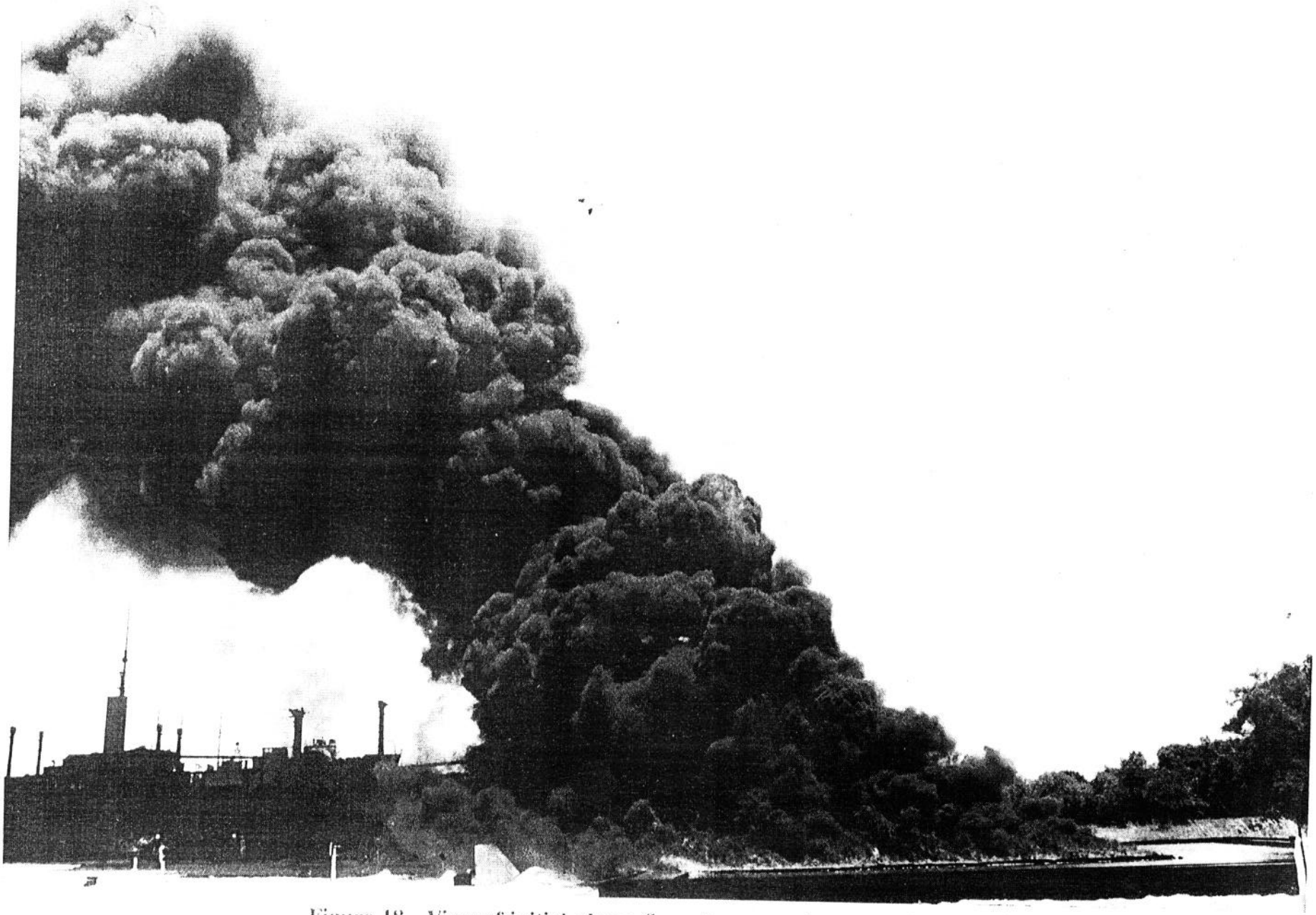

Figure 18. View of initial plume flow above pan in mesoscale burn 5/30

local particle deposition. Only a few percent of the ground level computational cells are actually occupied by particles. Again, the reader should be aware of the difference between the crosswind and downwind length scales when studying this figure.

Future work will focus on incorporating a more realistic description of the plume environment into the model. The atmospheric wind and temperature profiles will be made more realistic and some attempt to incorporate terrain effects into the model will be made. This will ultimately require an interface between this computer code and a local to regional scale meteorology model. The computational task will undoubtedly be larger than that presently required, but that should be more than offset by the explosive growth of inexpensive computing power.

SMOKE PLUME TRAJECTORY MODELING - EPA SCREEN MODEL

The NIST LES model provides detailed information on the plume trajectory, dispersion, and particulate deposition. The initial trajectory of the smoke plume agreed with measurements, but measurements were only obtained over a small portion of the predicted distance of the plume. No measurements of long range particulate deposition were attempted in the mesoscale burns, so these predictions remain unvalidated. Even though experimental measurements are not available, it is interesting to compare predictions of the NIST LES model to the widely used, and EPA approved, SCREEN model [23].

SCREEN is based on the classical diffusion equation, and thus provides near Gaussian distribution of combustion product concentration at specified locations downwind from the source as a function of a variety of input parameters, including wind speed, atmospheric stability class (an indicator of atmospheric turbulence based on solar elevation angle, cloud cover, cloud ceiling height and wind speed), particulate emission rate, and total heat release rate. SCREEN can run a full range of meteorological conditions, which consists of various combinations of wind speed and stability class.

SCREEN has three ways to specify the emission, including the point source, area source and flare source options. While none of them is exactly suited to predictions of large pool fires, the flare option furnishes the best means for simulating the burn. Although SCREEN was originally designed for modelling smoke plumes generated by low-energy (low-buoyancy) fires emitted from smoke stacks, it may be adaptable to high-energy crude oil fires as long as the user provides a realistic value for the heat release rate.

Results of the SCREEN calculations are subject to the following conditions that are built in assumptions of the model:

> With the flare option, plume rise is calculated from the top of the flame (the effective release height); the flame is assumed to be bent at a 45 degree angle.

Heat loss by radiation is 55% of the total heat released; the remaining 45% becomes the convective heat release used in the calculations. (In the LES model calculation the radiative loss was set at 40% which is generally used for highly radiative flames).

With the choice of the flare option, the following values are automatically assigned by the model:

Effective gas exit velocity = 20 m/s
Effective gas exit temperature = 1273 K
Ambient air temperature = 293 K

Once the stability class and wind speed are specified, they are assumed to obtain over the length of the plume; atmospheric inversions cannot be treated.

SCREEN has been used to model the smoke plume flow for the mesoscale burn 5/30. The parameter values used in the calculation are the following:

Smoke particulate emission rate = 0.5 kg/s (smoke particulate).

Flare stack height = 0.0 (ground level burn).

Effective release height = 20.48 m (the calculated height of the flame top).

Total heat release = 245 MW (based on an effective heat of combustion of 41.9 MJ/kg); 45% of this value (110 MW) is the convective heat release rate.

Receptor height = varied.

Based on the weather conditions at the test site, stability class C (strong incoming solar radiation, surface wind speed of 6 m/s) was assumed (see figure 18).

The results of the modelling run are presented in figures 19 through 21.

Figure 19 shows the downwind variation of maximum smoke concentration at ground level. These values occur below the plume centerline only and represent an average taken over one hour. As it is presently constituted, SCREEN has no means for calculating the settling out and subsequent ground deposition of smoke particulates. It assumes that the smoke is carried downstream as a neutrally buoyant mass that diffuses vertically and laterally in a Gaussian manner about the plume centerline. In addition SCREEN provides predictions for a maximum of 100 km downwind. The predicted ground level concentrations if interpreted as a deposition are much lower

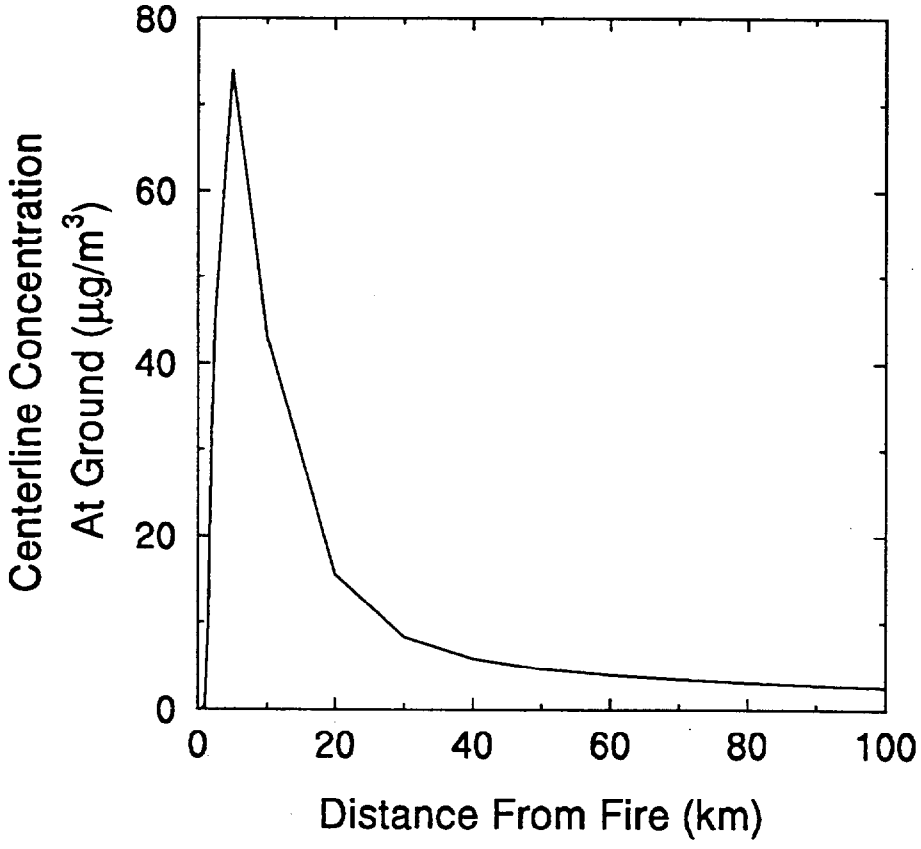

Figure 19. Screen prediction of ground level smoke particulate concentration

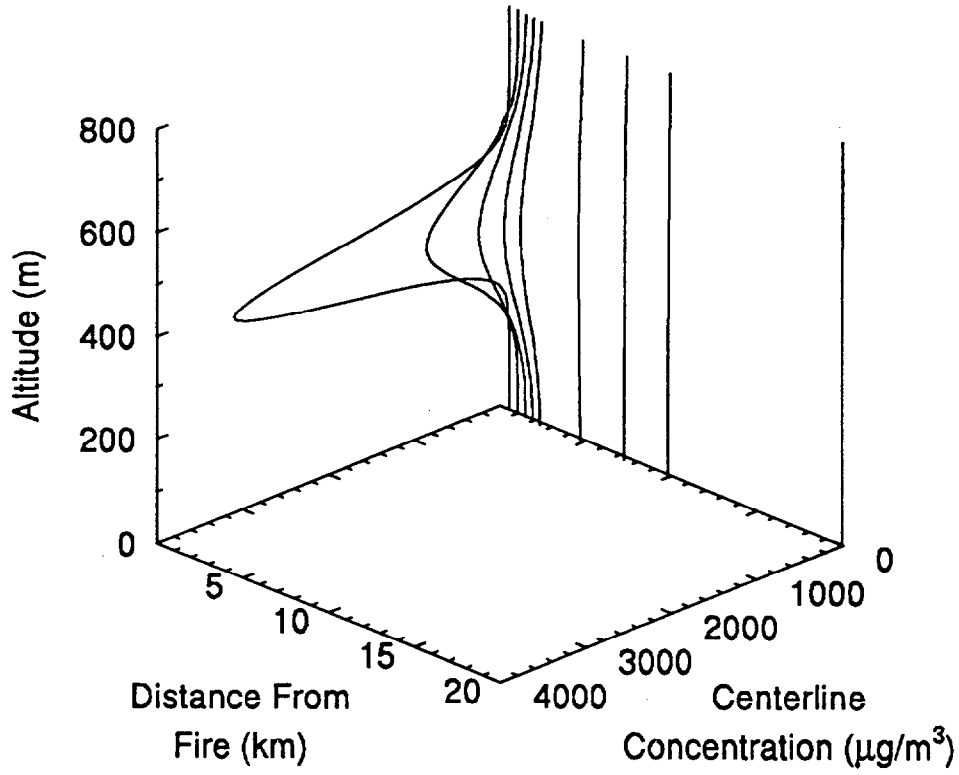

Figure 20. Screen prediction of smoke particulate concentration in air

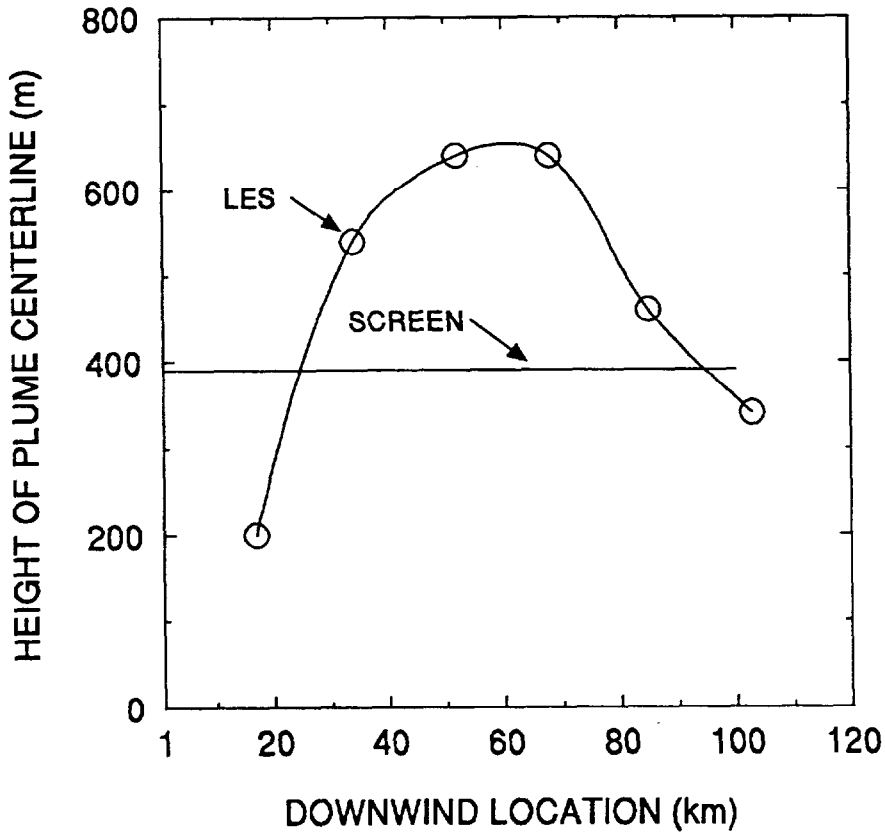

Figure 21. SCREEN and LES predictions of centerline plume height

than would be expected from the results of the LES model which predicts an average deposition of 1.5 mg/m^2. The smoke diffusion process is best illustrated in figure 20, which shows the vertical dispersion of smoke about the plume centerline with downwind distance; it is clear that most of the smoke is still well above ground, even far downwind. Finally, figure 21 shows the smoke plume height as a function of distance downwind. SCREEN is incapable of calculating the actual rise trajectory of the smoke plume and provides only a final constant plume height as compared to the rise and fall of the smoke plume predicted by LES.

CONCLUSIONS

For the mesoscale experiments, the average burning rate for fresh Louisiana crude oils at 17.2 m effective diameter was only 7% greater than that measured at the largest laboratory scale of 2.0 m. This indicates that with small corrections the burning rates of large laboratory fires can be used to estimate the expected steady burning of larger fires. The wind speed did not appear to affect the average burning rate but did contribute to variations in burning extinction. The recommended value to use for the burning rate of thick layers of fresh crude oils on water is 0.047 ± 0.01 kg/s/m^2 (4.9 ± 1 gal/hr/ft^2).

It was generally found that well over 90 percent of the fresh oil was consumed in the pan burns. In addition, the residue from the primary burn could be corralled and burned with the addition of a kerosene as an ignitor.

Smoke yield from fresh crude oil fires depends on diameter. In 0.085 m diameter laboratory fires the minimum smoke yield of 0.05 for Murban and 0.06 for Louisiana crude oils were measured. At 2.0 m diameter the smoke yield for the Murban crude oil was a significantly greater, 0.14, as measured in the large laboratory pan burns at FRI. Measurement from the mesoscale experiments are more scattered than the laboratory measurements, but the value of 0.13 ± 0.01 smoke yield represents most of these measurements. The recommended value for smoke yield from large the burning of thick layers of fresh Louisiana crude oil is 0.13. From laboratory burns it is expected that the Murban crude oil would have a higher smoke yield than the Louisiana crude oil if burned at mesoscale.

The size distributions of aerodynamic effective diameters for the smoke particulate were measured in the 2.0 m diameter laboratory and mesoscale fires. Most of the particulate mass was below 10 μm in diameter as measured with a cascade impactor. There is a shift of particulate size distribution to larger size particles from the larger diameter fire.

Prediction of the smoke plume trajectory and particulate deposition show that because the smoke particulate is distributed over great distances from the fire, the local concentration beyond the near fire region (which is not calculated) is small. The results from the LES and SCREEN models indicate the strength of the LES model over the EPA approved SCREEN model for predicting particulate deposition. The

LES model was written specifically to be able to predict particulate deposition and requires substantial computer resources whereas the SCREEN model was developed as a screening tool for general emissions. The LES model allows particulate to settle and deposit on the ground whereas the SCREEN model does not. As a result, SCREEN predicts the maximum downstream concentration of product remains at fixed altitude and particulate only reaches ground level through diffusion. The product that reaches the ground does not deposit there but continues to diffuse downstream.

ACKNOWLEDGEMENTS

This work was a continuation of studies begun in 1985 as part of the Technology Assessment and Research Program for Offshore Minerals Operations managed by John Gregory and Ed Tennyson of Minerals Management Service. The research was funded jointly by the Minerals Management Service, U.S. Department of the Interior, the American Petroleum Institute, and the U.S. Coast Guard, Department of Transportation. Special technical assistance and cooperation was provided by Merv Fingas of the Technology Development and Technical Services Branch, Environment Canada and the Rod Terpin of the Environmental Protection Agency, Emergency Response Team in Edison, NJ.

In connection with the experiments at FRI in Japan, we would like to acknowledge Dr. Tokio Morikawa for his analysis of CO_2 and CO content in the bag samples collected by the portable smoke sampler and Dr. Hashimoto from Tokyo Science University for analysis of smoke samples which yielded the electron microscope pictures of smoke particulate used in this paper.

The design and construction of a custom laser extinction meter to perform smoke measurements in the FRI facility by William Twilley was an outstanding example inventiveness and quality workmanship.

The cooperation and hospitality of the U.S. Coast Guard Research and Development Center and the Fire and Safety Test Detachment in preparing for and conducting the mesoscale burning experiments has been outstanding in every respect.

Donations of crude oil for the mesoscale experiments were made by Exxon Baton Rouge Refinery and BP America. Special measurement, testing, and analysis equipment in addition to profession staff time were provided to this project by EPA-ERT, ACS, 3M, NOAA, LSU.

Dr. James Morehart formerly of the Building and Fire Research Laboratory, NIST provided essential assistance in the design of measurement methods and analysis of the data from the mesoscale experiments. Richard Peacock contributed substantially to the analysis of burning rate data from the mesoscale burns.

William Twilly, Jay McElroy, and Roy McLane of the Building and Fire Research Laboratory, NIST provided immeasurable assistance in conducting the mesoscale burns.

Edward Budnick and Jerry Back of Hughes Associates provided detailed measurements and analysis of the smoke plume trajectories and shapes that were needed as part of the evaluation of the two predictive models for smoke dispersion.

Dennis Atkinson of the Source Receptor Analysis Branch, EPA and Dr. David O'Brien of North American/EMCON, Inc. provided valuable assistance in the operation of the SCREEN model.

The program of mesoscale burn experiments was coordinated through the Burn Evaluation Steering Team (BEST).

REFERENCES

1. Smith, N.K. and Diaz, A., In-place burning of Prudhoe Bay Oil in broken ice. Proceedings 1985 Oil Spill Conference, Prevention, Behavior, Control, Cleanup. pp. 405-410, 1985.

2. Tennyson, E.J., Results from Selected Oil Spill Response Research by the Minerals Management Service - Marine Technology Society Journal Volume 24 Number 4, pp 27-32, 1990

3. Brown, H.M. and Goodman, R.H., "In Situ Burning of Oil in Ice Leads," Proceedings of the Ninth Annual Arctic and Marine Oilspill Program Technical Seminar, June 10-12, 1986, Edmonton, Alberta, Canada, Environment Canada, Ottawa K1A 0H3, pp. 245-256, 1986.

4. Buist, I.A., and Twardus, E.M., "Burning Unconfined Oil Slicks: Large Scale Tests and Modelling," Proceedings of the Eighth Annual Arctic Marine Oilspill Program Technical Seminar, June 18-20, 1985, Edmonton, Alberta, Canada, Environment Canada, Ottawa K1A 0H3, pp. 103-130, 1985.

5. Evans, D., Baum, H., McCaffrey, B., Mulholland, G., Harkleroad, M., and Manders, W., "Combustion of Oil on Water," Proceedings of the Ninth Arctic Marine Oilspill Program Technical Seminar, June 10-12, 1986, Edmonton, Alberta, Ministry of Supply and Services Canada Cat. No. En 40-11/5-1986E, pp. 301-336, 1986.

6. Evans, D., Mulholland, G., Gross, D., Baum, H., and Saito, K., "Environmental Effects of Oil Spill Combustion," Proceedings of the Tenth Arctic and Marine Oilspill Program Technical Seminar, June 9-11, 1987, Edmonton, Alberta, Ministry of Supply and Services Canada Cat. No. En 40-11/5-1987E, pp. 91-130, 1987.

7. Evans, D., Mulholland, G., Gross, D., Baum, H., and Saito, K., "Burning, Smoke Production, and Smoke Dispersion from Oil Spill Combustion," Proceedings of the Eleventh Arctic and Marine Oil Spill Program Technical Seminar, June 7-9, 1988, Vancouver, British Columbia, Ministry of Supply and Services Canada, Cat. No. En 49-11/5-1988 E/F, pp. 41-87, 1988.

8. Evans, D., Baum, H., Mulholland, G., Bryner, N., and Forney, G., "Smoke Plumes From Crude Oil Burns," Proceedings of the Twelfth Arctic and Marine Oil Spill Program Technical Seminar, June 7-9, 1989, Calgary, Alberta, Ministry of Supply and Services Canada, Cat. No. En 40-11/5-1989, pp. 1-22, 1989.

9. Evans, D., Walton, W., Baum, H., Lawson, R., Rehm, R., Harris, R., Ghoniem, A., Holland, J., "Measurement of Large Scale Oil Spill Burns," Proceedings of the Thirteenth Arctic and Marine Oil Spill Program Technical Seminar, June 6-8, 1990, Edmonton, Alberta, Ministry of Supply and Services Canada, Cat. No. En 40-11/5-1990. pp. 1-38, 1990.

10. Benner, B. A. Jr., Bryner, N. P., Wise, S. A., Mulholland, G. W., Lao, R. C., Fingas, M. F., "Polycyclic Aromatic Hydrocarbon Emissions from the Combustion of Crude Oil on Water," Environmental Sciences & Technology, Vol. 24, pp. 1418-1427, 1990.

11. Evans, D., Walton, W., Baum, H., Mulholland, G., Lawson, J., Koseki, H., Ghoniem, "Smoke Emission from Burning Crude Oil," Proceedings of the Fourteenth Arctic and Marine Oil Spill Program Technical Seminar, June 12-14, 1991, Vancouver, British Columbia, Ministry of Supply and Services Canada, Cat. No. En 40-11/5-1991. pp. 421-449, 1991.

12. Evans, D., Tennyson, E.J., In-Situ Burning -- A Promising Oil Spill Response Strategy, Seventh Symposium on Coastal and Ocean Management, July 8-12, 1991, Long Beach, California, conference preprint, 1991.

13. Babrauskas, V., The Cone Calorimeter -- A New Tool for Fire Safety Engineering, ASTM Standardization News, Vol 18, pp. 32-35, 1990.

14. Mulholland, G.W., Henzel, V., Babrauskas, V., The Effect of Scale on Smoke Emissions, Fire Safety Science -- Proceedings of the Second International Symposium, Hemisphere Publishing Corporation, New York, pp.347-357, 1989.

15. Babrauskas, V., Mulholland, G., Smoke and Soot Data Determinations in the Cone Calorimeter, Mathematical Modeling of Fires, ASTM STP 983, American Society for Testing and Materials, Philadelphia, pp. 83-104, 1987.

16. Hering, S.V. (editor), Air Sampling Instruments for Evaluation of Atmospheric Contaminates, 7th Edition, American Conference of Governmental Industrial Hygienists, Cincinnati, Ohio, 1989.

17. Marple Personnel Cascade Impactors, Series 290, Instrument Manual, Bulletin No. 290I.M.-3-82, Sierra Instruments, Inc, Carmel Valley, CA.

18. Pagni, P.J., Fire Modeling, Grant Report, Summaries of BFRL Fire Research Program In-House Projects and Grants, 1991, Nora Jason, Editor, National Institute of Standards and Technology, Gaithersburg, MD, pp.57-60, 1991.

19. Hamins, A., Yang, J.C., Kashiwagi, T., An Experimental Investigation of the pulsation Frequency of Flames, 24th Symposium (International) on Combustion, The Combustion Institute, Pittsburgh, PA., to appear.

20. Gengembre, E., Cambray, P., Karmed, D., Bellet, J.C., Turbulent Diffusion Flames with Large Buoyancy Effects, Comb. Sci. Tech. 41, 55,1984.

21. Leonard, J.T., Budnick, E.K., Back, G.G., Garney, S.J., Development of a Video Image-based Methodology for Estimating Large Scale Hydrocarbon Smoke Plume Size and Extent, Naval Research Laboratory, in preparation.

22. Rehm, R.G., Tang, H.C., Baum, H.R., Sims, J.S., and Corley, D.M., A Boussinesq Algorithm for Enclosed Buoyant Convection in Two Dimensions, NISTIR 4540, National Institute of Standards and Technology, Gaithersburg, MD, 1991.

23. Brode, Roger W., Screening Procedures for Estimating the Air Quality Impact of Stationary Sources, EPA-450/4-88-010, U.S. Environmental Protection Agency, Research Triangle Park, N.C., 1988.

Environment Canada. Arctic and Marine Oilspill Program Technical Seminar, 15th. June 10-12, 1992, Edmonton, Canada, Environment Canada, Ottawa, Ontario, 593-657 pp, 1992.